Analytica Chimica Acta 737 (2012) 1–21

Contents lists available at SciVerse ScienceDirect

Analytica Chimica Acta

journal homepage: www.elsevier.com/locate/aca

Review

Recent advances in ZnO nanostructures and thin films for biosensor applications: Review

Sunil K. Arya[a,*], Shibu Saha[b], Jaime E. Ramirez-Vick[c], Vinay Gupta[b], Shekhar Bhansali[d], Surinder P. Singh[e,**]

[a] Bioelectronics Program, Institute of Microelectronics, A*Star 11 Science Park Road, Singapore Science Park II, Singapore 117685, Singapore
[b] Department of Physics & Astrophysics, University of Delhi, Delhi 110007, India
[c] Engineering Science & Materials Department, University of Puerto Rico, Mayaguez, PR 00681, USA
[d] Department of Electrical and Computer Engineering, Florida International University, Miami, FL, USA
[e] National Physical Laboratory, Dr K.S. Krishnan Marg, New Delhi 110012, India

HIGHLIGHTS

- This review highlights various approaches to synthesize ZnO nanostructures and thin films.
- Article highlights the importance of ZnO nanostructures as biosensor matrix.
- Article highlights the advances in various biosensors based on ZnO nanostructures.
- Article describes the potential of ZnO based biosensor for new generation healthcare devices.

GRAPHICAL ABSTRACT

ZnO nanostructures have shown binding of biomolecules in desired orientation with improved conformation and high biological activity, resulting in enhanced sensing characteristics. Furthermore, their compatibility with complementary metal oxide semiconductor technology for constructing integrated circuits makes them suitable candidate for future small integrated biosensor devices. This review highlights various approaches to synthesize ZnO nanostructures and thin films, and their applications in biosensor technology.

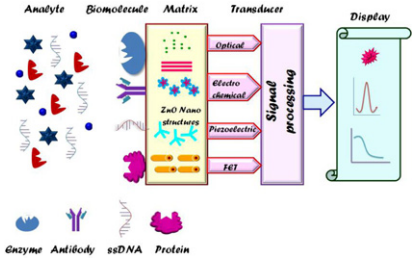

ARTICLE INFO

Article history:
Received 5 December 2011
Received in revised form 25 May 2012
Accepted 28 May 2012
Available online 4 June 2012

Keywords:
ZnO nanostructures
Biosensor
Nanorods
Nanoflowers
Electrochemical

ABSTRACT

Biosensors have shown great potential for health care and environmental monitoring. The performance of biosensors depends on their components, among which the matrix material, i.e., the layer between the recognition layer of biomolecule and transducer, plays a crucial role in defining the stability, sensitivity and shelf-life of a biosensor. Recently, zinc oxide (ZnO) nanostructures and thin films have attracted much interest as materials for biosensors due to their biocompatibility, chemical stability, high isoelectric point, electrochemical activity, high electron mobility, ease of synthesis by diverse methods and high surface-to-volume ratio. ZnO nanostructures have shown the binding of biomolecules in desired orientations with improved conformation and high biological activity, resulting in enhanced sensing characteristics. Furthermore, compatibility with complementary metal oxide semiconductor technology for constructing integrated circuits makes ZnO nanostructures suitable candidate for future small integrated biosensor devices. This review highlights recent advances in various approaches towards synthesis of ZnO nanostructures and thin films and their applications in biosensor technology.

* Corresponding author. Tel.: +65 90702464.
** Corresponding author.
E-mail addresses: sunilarya333@gmail.com (S.K. Arya), singh.uprm@gmail.com, singhsp@mail.nplindia.ernet.in (S.P. Singh).

0003-2670/$ – see front matter © 2012 Elsevier B.V. All rights reserved.
http://dx.doi.org/10.1016/j.aca.2012.05.048

Contents

Sunil K. Arya received BSc in chemistry in 2002, MSc in organic chemistry in 2004 and PhD in chemistry-biosensor in 2008 from the University of Delhi, Delhi, India. He is currently a scientist at Institute of Microelectronics, A*star, Singapore. He has completed a post doctorate at University of South Florida, Tampa, Florida, USA and at National Institute of Nanotechnology and university of Alberta, Edmonton, Alberta, Canada. His primary interests are in synthesis and applications of Nanomaterials, monolayers and MEMS for gas sensor and electrochemical biosensor. His research focus is in the areas of micro/nanofabrication, materials science and thin film sensors/biosensor.

Shibu Saha received his BSc and MSc degrees in physics in the year 2004 and 2006 respectively, from University of Delhi. He submitted his PhD thesis at University of Delhi, Delhi. His research interests are in the field of biosensors including sensor characterization, growth and study of metal oxide films.

Jaime E. Ramirez-Vick is professor and director of the Engineering Science & Materials Department at the University of Puerto Rico–Mayaguez (UPRM). He has graduate and undergraduate degrees in chemical engineering from UPRM and Arizona State University, with postdoctoral training at the Lawrence Berkeley National Laboratory and the Cancer Center of the University of California–San Francisco. His research interests include the development of protein and nucleic detection electrochemical biosensors based on thin films and nanostructures.

Vinay Gupta born in Mujjaffar Nagar (U.P.), India, (March, 1967) received his BSc, MSc and PhD degrees in physics in 1987, 1989 and 1995, respectively from the University of Delhi, India. Subsequently he joined DDU College, University of Delhi as assistant professor. Presently he is professor in the Department of Physics and Astrophysics, University of Delhi, India. He is a senior member of IEEE. His current research interests are in the field of growth and characterization of piezoelectric, ferroelectric and semiconducting thin films for their application in gas/bio sensors, Electro-optic studies, oxide nanostructures for multifunctional applications, etc.

Shekhar Bhansali is aAlcatel–Lucent professor and chair in the Department of Electrical and Computer Engineering at the Florida International University. He received his PhD in electrical engineering (1997) from Royal Melbourne Institute of Technology, Melbourne, Australia. His interests are in the areas of Bio-MEMS, sensors, nanostructures and Microsystems. He is the recipient of NSF CAREER Award, Alfred P. Sloan Foundation Outstanding Mentor Award, FGLSAMP Outstanding Mentor Award, FEF Outstanding Mentor Award and USF Outstanding Researcher Award. He holds 11 patents in the area of biosensors, nanostructures and Microsystems technologies, has co-authored over 170 journal and conference publications and is editor of the book "MEMS for biomedical Applications", to be released in Fall 2012.

S.P. Singh obtained his MSc (1992) and PhD (1998) degrees from G.B. Pant University of Agriculture & Tech., Pantnagar, India, in Physics. He is working as a scientist at the National Physical Laboratory, New Delhi, India. He served as assistant professor at University of Puerto Rico, Mayaguez, USA, 2008–2011. His research is focused on nanomaterials, nanomedicine, nanobiointerface, bio-implants, biosensors for healthcare and Gas sensors.

1. Introduction

Recent advances in interdisciplinary research and molecular diagnostics have led to the rapid development of different classes of biosensors for a wide range of bioanalyte detection with improved sensing characteristics. In addition, continuous developments in the fields of engineering and nanotechnology have contributed to miniaturization and multifunctionality in biosensor technology. A schematic of a biosensor shown in Fig. 1 clearly indicates that sensing biomolecules need to be integrated into the system on a solid support. The type of solid support that holds the sensing biomolecule (receptor) is known as a matrix. A suitable matrix enhances signal transduction and helps to immobilize biomolecules with retained or enhanced activity. The physico-chemical properties of the matrix dictate the method of immobilization and the operational stability of the biosensor [1]. Moreover, the matrix alters the resistance of the biomolecule to various physical and chemical changes, such as pH, temperature and chemical composition changes. Recently, ZnO thin films and nanostructures have gained much attention as a suitable matrix for biomolecule binding. This review is intended to comprehensively report on recent advances in the synthesis protocols of various ZnO nanostructures and thin films in addition to the applications of ZnO structures in biosensors.

1.1. Zinc oxide

ZnO is a well-known n-type, direct wide-band-gap II–VI semiconductor with band gap of 3.37 eV and a large excitonic binding energy of 60 meV at room temperature [2–4]. The direct wide-band-gap of ZnO makes the semiconductor a good candidate for optoelectronic applications and the large exciton energy helps to employ the excitonic recombination process as a lasing mechanism [5]. ZnO is a polar semiconductor material with two crystallographic planes that have opposite polarity and different surface relaxation energies, which lead to a higher growth rate along the *c*-axis, e.g., the formation of nanorod-like vertical structures [6]. ZnO exists in wurtzite and zinc-blende crystal structures (Fig. 2) [7]; however, at ambient temperature and pressure, ZnO crystallizes normally in a wurtzite structure with a hexagonal lattice that has two interconnecting sub-lattices of Zn^{2+} and O^{2-} with the zinc ion surrounded by tetrahedral oxygen ions and vice versa. This tetrahedral coordination gives rise to a polar symmetry along the hexagonal axis, which is responsible for a number of the physical and chemical properties of ZnO, including piezoelectricity and spontaneous polarization. The structure of ZnO is a key factor in crystal growth, etching and defect generation. The large piezoelectric coefficient of ZnO has allowed for the development of surface acoustic wave (SAW) devices that can operate at higher frequencies than other devices. The variation in electrical properties such as conductivity is dictated by the presence of oxygen vacancies, shallow zinc interstitial, hydrogen impurity and other donor type point defects. Moreover, the ZnO near-surface region can be highly conductive due to H donors in this region and a large density of near-surface electrons.

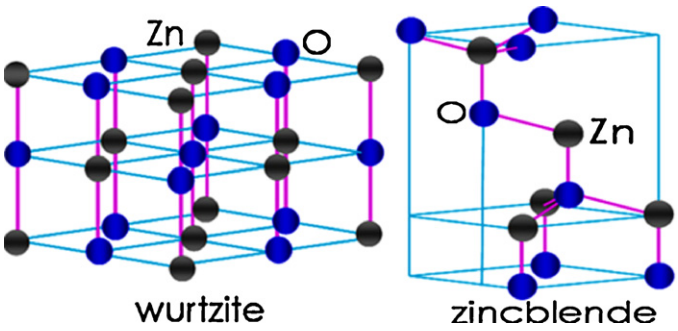

Fig. 2. Schematic representation of ZnO crystal structures: wurtzite and zinc blende [7].

From a technological viewpoint, ZnO is an important, multifunctional material with a number of applications in transparent electronics, smart windows, piezoelectric devices, UV-lasers, UV-photodetectors, gas sensors, chemical sensors, biosensors and dye-sensitized solar cells [3,8–12]. In addition, the ferromagnetic properties of "rare-earth metals" doped ZnO show potential for spintronic based devices. Further, due to its biocompatibility, in addition to its antibacterial and other novel properties, ZnO has been utilized in a variety of applications, such as drug

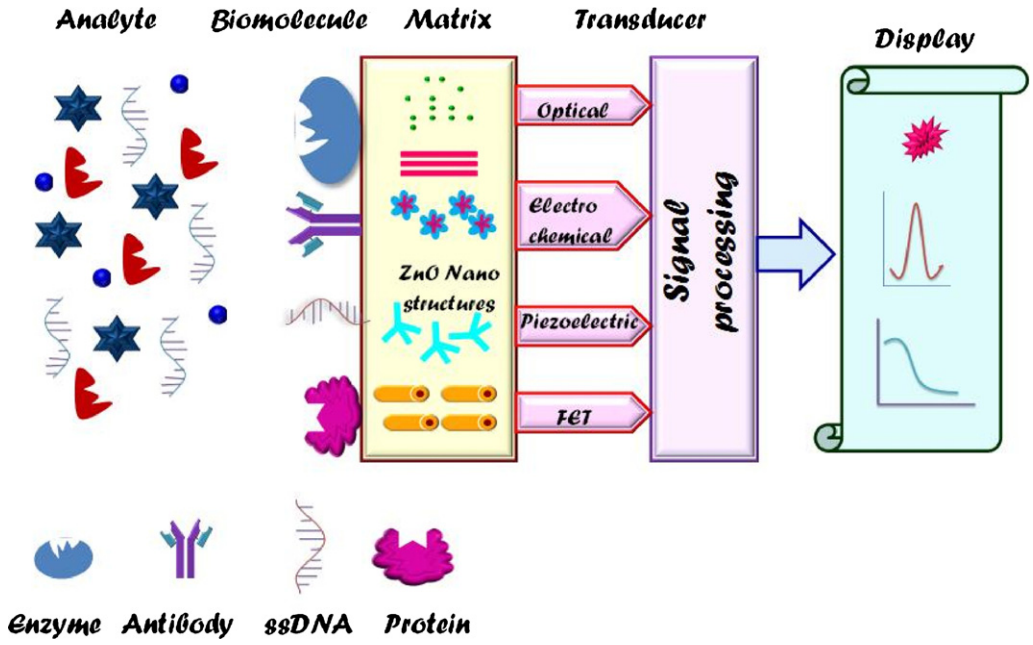

Fig. 1. Schematic of biosensor assembly.

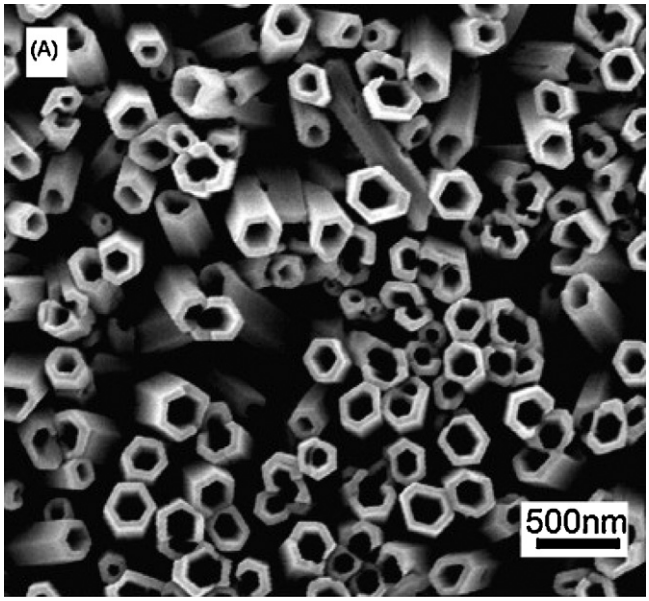

Fig. 3. FESEM images of ZnONT [43].

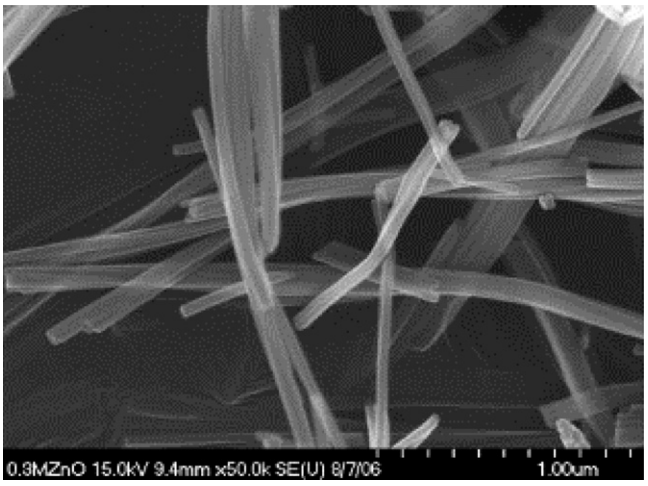

Fig. 4. FESEM images of ZnO nanobelt [45].

delivery, cancer treatment, bio-imaging, medical products, sunscreens, skin lotions, etc. [13–17]. The excellent electron communication ability, and chemical stability with high isoelectric point (approximately 9) makes ZnO an attractive matrix for biosensor applications [18]. Further, these characteristics can be modified through the chemical functionalization of the ZnO surface. In addition, ZnO films can be prepared by methods amenable to large-scale manufacturing at temperatures that allow for low-cost operation and flexible substrates [19]. Finally, thin films of ZnO offer the advantage of monolithic integration with advanced complementary metal-oxide-semiconductor (CMOS) technology for highly sensitive and selective chemical and/or biological sensor arrays [2].

1.2. ZnO nanostructures in biosensors

In recent years, nanostructured ZnO for biosensing applications has attracted great interest compared to bulk ZnO films [20–23]. Nanostructures offer numerous unique features and show great promise for faster responses and higher sensitivity than planar sensor configurations. Due to their small dimensions, increased sensing surface and strong binding properties, nanoscale ZnO structures can achieve single-molecule detection. Interestingly, ZnO can be grown to form highly anisotropic nanostructures on various substrates including sapphire, glass, silicon and conductive surfaces (e.g., indium-tin-oxide (ITO), gold) with different morphologies [5,24]. ZnO nanomaterials can act as excellent fluorescence-enhancing substrates for the detection of biomolecules [25]. In addition, ZnO quantum dots (QDs), are excellent quantitative labels for biological assays based on their high aspect ratio and substantial optical and electronic signal amplification [26].

Researchers have studied myriad of ZnO nanostructures for biosensor applications that are synthesized by various physical and chemical routes. These nanostructures include wires (ZnONW) [14,23,24,27,28], rods (ZnONR) [25,29,30], combs [31,32], forks [33], fibers [20], flakes [21], waxberries [34], bundles [35], spheres [22], composites [36], tetrapods [37,38], particles (ZnONP) [39–41], nanorod spheres [42], tubes (ZnONT) (Fig. 3) [43,44], belt (Figs. 4 and 5) [45,46] flowers (Figs. 6 and 7) [47–49] and sheets/disks (Fig. 8) [50–52]. In addition to their great potential for fundamental studies on the roles of dimensionality and size based physical properties, ZnO nanostructures have received considerable interest as building blocks and interconnections for electronic and photonic devices as well as sensors [33]. Nanoporous and nanostructured ZnO films have also been used for biosensor applications [53–55]. The ease of fabrication using low cost processes, which can yield a wide range of nanostructures, makes ZnO-based matrices a promising platform for low cost biosensors. Further characterization of these nanostructured materials is essential to advance the field of electrochemical biosensors and reach the goal of a sensitive, fast and inexpensive point-of-care diagnostic device. The following sections describe the details of various synthesis processes used for the preparation of these nanostructures.

2. Synthesis of ZnO nanostructures

The physical and chemical properties of nanomaterials vary as a function of size, shape and surface chemistry. Thus, new synthetic strategies are vital for the development of novel nanomaterials. Generally, the synthesis methods for ZnO nanostructures can be divided into two groups: wet-chemical/solution based and physical techniques based [33]. Physical techniques, such as vapor–liquid–solid (VLS), vapor solid and chemical vapor deposition (CVD) in addition to thermal evaporation, typically require high temperatures and pressures as well as particular substrates and result in low product yield. These methods produce high-quality ZnO nanostructures; however, the methods are energy and cost intensive.

Wet-chemical/solution based methods include hydrothermal/solvothermal processes, solution–liquid–solid (SLS) and capping agents/surfactant-assisted synthesis. Zinc readily forms hydroxy and ammonia complexes and these methods are based on the hydrolysis of such complexes at elevated or room temperatures. Further, the growth direction can be controlled with various additives in these methods. Amine compounds are often used to direct growth in the *c*-direction, whereas citrate inhibits *c*-direction growth and directs the crystal shape into thicker rods or even plates. Thus, wet-chemical/solution based methods provide convenient, facile manipulation, potential for scale-up and a lower temperature pathway for the fabrication of the desired ZnO nanostructures [28,33,56–59]. Among these methods, the solution based method via seed layer deposition followed by ZnO growth is the most common procedure for growing nanostructures. Recently, electrochemical techniques have also emerged as a new synthesis method for ZnO nanostructures [20,28,43].

Table 1
Summary of various wet chemical approaches for ZnO nanostructure synthesis.

Structure type	Matrix	Seed layer	Growth reagent	Growth condition	Reference
ZnONR	Ag wire	$Zn(CH_3COO)_2$	$Zn(NO_3)_2$ & HMTA	Incubation at 90 °C, 2 h	[67]
ZnONR	ITO	ZnONP	$Zn(NO_3)_2$ & HMTA	Incubation at 90 °C, 3 h	[29]
ZnONR	Au wire	Zinc	Zinc solution	Autoclave at 85 °C, 20 h	[69]
ZnONR	Au	–	$ZnCl_2$ & NH_3	95 °C, 90 min in oven	[31,70]
ZnONR	Quartz crystal	ZnO	$Zn(NO_3)_2$, pH 10.6	90 °C, 1–3 h	[79]
ZnONR	Silicon		$Zn(NO_3)_2$ & HMTA	Autoclave at 95 °C, 7 h	[30]
ZnONR	Nanocrystalline diamond	ZnO	$Zn(NO_3)_2$ & HMTA	Incubation at 70 °C, 8 h	[25]
ZnO nanofork, nanobundles and nanorods	In solution	–	$Zn(CH_3COO)_2$& citric acid	(i) Incubation at 80 °C, 9 h, (ii) calcination 400 °C, 2 h	[33,35,76]
ZnO nanoflower	In solution	–	$ZnCl_2$, PVP, glycol, NaOH & ascorbic acid	(i)55 °C, 3 h, (ii) drying at 150 °C	[47]
ZnO nanoflower	In solution	–	$Zn(CH_3COO)_2$& NaOH	(i) Autoclave at 180 °C, 13 h, (ii) drying at 100 °C 4 h	[71–73]
ZnO nanoflower, nanobelt	In solution	–	$Zn(CH_3COO)_2$& NaOH	Reflux at 90 °C, 1 h	[45]
ZnO nanoflower	In solution	–	$Zn(NO_3)_2$, NaOH & hydroethylenediamine	(i) Ultrasonication, 30 min (ii) autoclave at 180 °C, 15 h	[49]
ZnO nanoflowers	In solution	–	$Zn(NO_3)_2$ & HMTA, pH 10	Reflux at 100 °C, 9 h	[48]
ZnONW	Ag wire	$Zn(NO_3)_2$ & HMTA	$Zn(NO_3)_2$ & HMTA	Heating at 90 °C	[79]
ZnONW	Tantalum foil	ZnO	$Zn(OH)_4^{2-}$, pH 12–14	Autoclave 100 °C, 24 h	[23]
ZnONW	Fe–Co–Ni alloy	–	$Zn(NO_3)_2$ & NH4OH	Heating at 70 °C, 24 h	[56,85]
ZnONP	In solution	–	$Zn(CH_3COO)_2$, HMTA & LiOH, pH 10	Reflux at 90 °C, 3 h	[86]
ZnONP	In solution	–	$Zn(NO_3)_2$ & NaOH	Heating at 80 °C, 6 h	[87]
ZnONP	In solution	–	$Zn(NO_3)_2$ & diethylaminetriamine	Heating at 95 °C, 3 h	[88]
ZnONP	In solution	–	$ZnCl_2$, hydroxypropyl cellulose & KOH	Heating at 60 °C, 2 h	[89]
ZnO nanosheet, microsphere	In solution		$Zn(NO_3)_2$, HMTA & trisodium citrate	(i) Heating at 95 °C, 35 min, (ii) annealing at 320 °C, 1 h	[50]
Rod constructed ZnO microsphere	In solution	–	$Zn(NO_3)_2$, NaOH, & Cetyl trimethylammonium bromide	Autoclave 120 °C, 3 h	[42]
ZnO nanoflakes	Aluminum	–	$Zn(NO_3)_2$ & HMTA	Heating at 90 °C, 4 h	[21]
Waxberry likeZnO microballs	In solution	–	$Zn(CH_3COO)_2$, PVP, glycol and $NaHCO_3$	Reflux for 24 h	[34]
ZnONR having VRHHPs	Glass	–	$Zn(CH_3COO)_2$ & NH_4OH, pH 12	(i) Heating at 90 °C, 1 h, (ii) Annealing at 250 °C	[3]
ZnO nanotetrapods	In solution	–	$ZnSO_4$, polyglycol & KOH	(i) KOH addition at 50 °C, (ii) Aging for 10 min at 50 °C	[38,75]
Disk like hierarchical ZnO	Silicon	–	$ZnCl_2$, $Zn(CH_3COO)_2$ & HMTA	Heating at 90 °C, 1 h	[31]
ZnO QD	In solution	–	$Zn(CH_3COO)_2$, LiOH	Heating at 80 °C, 2 h	[26,90]
ZnO-Au nanocomposite	In solution	–	$Zn(CH_3COO)_2$, LiOH, trisodium citrate & $HAuCl_4$	(i) Refluxing at 80 °C, 100 min, (ii) Stirring for 48 h	[36,91]
Fe_3O_4/ZnO/Au nanorice	In solution	Fe_3O_4	$Zn(CH_3COO)_2$, LiOH, Fe_3O_4, ethylene glycol & $HAuCl_4$	(i) Heating at 150 °C, 3 h, (ii) 80 °C, 30 min	[92]
ZnONR	Glass	–	$Zn(NO_3)_2$, NH_4OH & ethanolamine	Heating at 75 °C, 1.5 h	[93]
ZnONR	Silicon nitride	–	$Zn(NO_3)_2$ & HMTA	Heating at 95 °C, 3 h	[94]
ZnONW	Ag wire	$Zn(NO_3)_2$ & HMTA	$Zn(NO_3)_2$ & HMTA	Heating at 90 °C	[61,78,95]
ZnONT	Au/glass	$Zn(NO_3)_2$ & HMTA	$Zn(NO_3)_2$, HMTA	(i) 90 °C, 4–6 h, (ii) Etching in KCl at85 °C	[96]

Table 1 (*Continued*)

Structure type	Matrix	Seed layer	Growth reagent	Growth condition	Reference
ZnONP	In solution	–	$Zn(NO_3)_2$, NaOH	Heating for 2 h	[97–99]
ZnO nanowalls	Al wire	$Zn(NO_3)_2$ & HMTA	$Zn(NO_3)_2$, HMTA	Heating at 90 °C, 2.5 h	[100]
ZnONP	In solution	–	$Zn(NO_3)_2$, polyethylene glycol & KOH	Heating at 50 °C, 2 h	[101]
ZnONP	In solution	–	$Zn(CH_3COO)_2$, ethylene glycol	Refluxing at 160 °C, 12 h	[102]
Boron doped nanostructured ZnO film	ITO	–	$Zn(CH_3COO)_2$, 2-Methoxethanol, ethanolamine, trimethyl borate	(i) Heating at 60 °C, 2 h to make sol–gel (ii) 300 °C, 10 min (iii) 500 °C, 1 h	[103]
Nanostructured ZnO film	Silicon	–	$Zn(CH_3COO)_2$, 2-Methoxethanol, monoethanolamine	(i)300 °C, 10 min (ii)450 °C, 1 h (iii)750 °C, 1 h	[104]
ZnONR	Glass	Al doped ZnO	$Zn(CH_3COO)_2$ & HMTA	Autoclave 90 °C, 3 h	[105]
ZnO nanosheets	Glass microslide	–	$ZnSO_4$, NH_4OH, pH 11	24 h incubation	[106]
ZnO rod-assembled microsphere	In solution	–	$Zn(NO_3)_2$, NaOH & poly ethylene glycol	(i) Supersonic at 40 kHz, 10 min (ii) Autoclave 180 °C, 30 min in microwave hydrothermal system	[107]
Nanosized ZnO	In solution	–	$ZnSO_4$, NaOH	24 h incubation	[108]
Flowerlike ZnONRs	In solution	–	$Zn(CH_3COO)_2$ & NH_3	Autoclave 80 °C, 20 h	[109]
Fe-doped ZnO nanosheets	In solution	–	$Zn(NO_3)_2$, urea, ferric nitrate	(i) Autoclave 160 °C, 10 h (ii) Annealing 500 °C, 2 h	[110]
ZnO nanoflower	In solution	–	$Zn(CH_3COO)_2$ & KOH	180 W microwave radiation, 20 min	[111]
ZnONP	In solution	–	$Zn(NO_3)_2$, $(NH_4)_2CO_3$	Vigorous stirring Calcination 550 °C, 2 h	[112]
ZnO nanoflakes & nanoclumn	In solution	–	$ZnSO_4$, NaOH, NaF (nanoflakes) $Zn(CH_3COO)_2$, NaOH & glycerine (nanocolumn)	Autoclave 200 °C, 24 h (nanoflakes) Autoclave 150 °C, 24 h (nanocolumn)	[113]
ZnONP	In solution	–	$Zn(NO_3)_2$, NaOH	Heating at 55 °C, 2 h	[97]
ZnO nanotetragonal pyramid	In solution	–	$ZnSO_4$, polyglycol & KOH	Sonication at 50 °C	[38]
ZnO nanosphere	In solution	–	(A) [Zn(salen)], oleylamine	(A) (i) 170 °C, 90 min	[114]
ZnO nanobundles			(B) [Zn(salen)]	(ii) 240 °C, 70 min (B) 500 °C, 5 h	
ZnO/Cu nanocomposite	ITO	Cu–Zn alloy	Cu–Zn alloy coated ITO in DI water	Autoclave 90 °C, 18 h	[115]
Multi-petals ZnO nanostructures	In solution	–	$Zn(CH_3COO)_2$, NaOH & β-cyclodextrin	Heating at 90 °C, 1 h	[64]

Table 1 (*Continued*)

Structure type	Matrix	Seed layer	Growth reagent	Growth condition	Reference
3D-flowerlike ZnO micro-nanostructure	In solution	–	$Zn(NO_3)_2$, HMTA & ethylenediamine	Heating at 95 °C, 2 h	[65]
3D-flowerlike ZnO nanostructure	GaN	–	$Zn(CH_3COO)_2$, NH_4OH	Heating at 95 °C, 2 h	[116]
Flowerlike ZnO nanostructure	ITO	–	$Zn(NO_3)_2$, HMTA	Heating at 90 °C, 4 h	[117]
Flowerlike ZnO nanostructure	In solution	–	$Zn(NO_3)_2$, NH_3, glycol & ethylenediamine	Autoclave 90 °C, 20 h	[63]
Flowerlike ZnO nanostructure	$GaN/LiAlO_2$	–	$Zn(NO_3)_2$, HMTA	Heating at 90 °C, 1 h	[118]
Flowerlike ZnO nanostructure	In solution (reverse micelles)	–	$Zn(NO_3)_2$, triton X-100, cyclohexane, hexacohol & NH_3	(i) Autoclave 150 °C, 24 h (ii) Drying 70 °C, 10 h (iii) Calcinations 500 °C, 3 h	[84]
Microsphere ZnO nanostructures	In solution	–	$Zn(CH_3COO)_2$, DEA	(i) Heating at 60 °C, 1 h (ii) Room temperature aging, 1 h (iii) Autoclave 150 °C, 6 h	[62]
ZnO complex nanostructures	Glass	ZnO	$Zn(NO_3)_2$, HMTA & $Al(NO_3)_3$, pH 5	Autoclave 90 °C, 1–4 h	[81]
ZnONP	Glass fiber mat	–	$ZnCl_2$, polyvinyl alcohol	(i) Heating at 250 °C, 4 h (ii) Carbonization at 450 °C	[119]
ZnONP	In solution	–	$Zn(CH_3COO)_2$, NaOH & polyethylene imine	Ultrasonication, 10 min	[120]
ZnONR	In solution	–	$Zn(CH_3COO)_2$, ethylene diamine	(i) Reflux at 80 °C, 2 h (ii) Reflux at 80 °C, 30 min with $H_2C_2O_4.2H_2O$ (iii) Calcinations at 500 °C, 2 h	[121]
ZnO nanoneedle	In solution	–	$Zn(NO_3)_2$, NaOH & sodium dodecylsulphate	Autoclave 85 °C, 5 h	[122]
ZnONR	In solution (reverse micelles)	–	$Zn(CH_3COO)_2$, NaOH, triton X-100, cyclohexane, *n*-octanol	Autoclave 120 °C, 12 h	[123]
ZnO hollow nanosphere	In solution	–	$Zn(CH_3COO)_2$, carbon sphere	(i) Room temperature incubation, 24 h (ii) Drying at 60 °C, 6 h (iii) Calcinations 450 °C, 2 h	[82]
Dendritic ZnO nanostructure	In solution	–	$Zn(CH_3COO)_2$ & 1-(2-hydroxyethyl)-3-methylimidazo-lium tertrafluoroborate	High intensity ultrasonication (500 W, 40 kHz), 2 h, room temperature	[83]

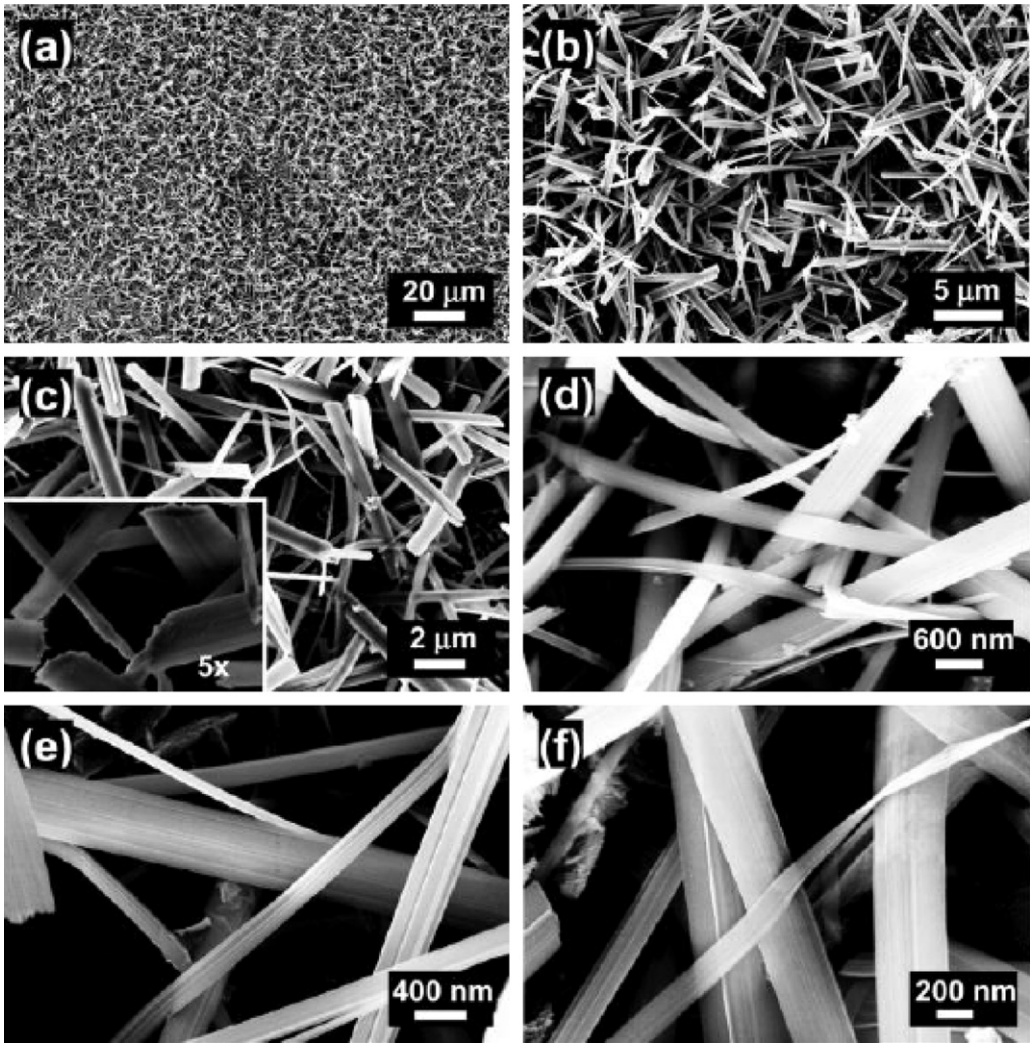

Fig. 5. SEM images of ZnO nanobelt-like structures electro-deposited onto a conducting PET substrate at 0 °C in 0.1 M $Zn(NO_3)_2{\cdot}6H_2O$ mixed with 0.1 M KCl electrolyte for 180 min [46].

2.1. Wet-chemical/solution based approaches

The solution based approach has gained much interest compared to other techniques for ZnO nanostructure growth. In this approach, morphological and structural characteristics of the grown ZnO nanostructures can be controlled by adjusting the growth process parameters, such as the reagent of interest, stoichiometry, temperature and pH [60,61]. Further, alcohol molecules, such as those in ethanolamine family (growth-directing), or stabilizing solvents play the vital role of contributing unoccupied oxygen to Zn^{2+} to form ZnO [62]. Using different amine precursors and surfactant-free hydrothermal processes various controllable ZnO architectures, such as flower-like structures radially assembled by rods, nails or towers and radialized bundled tubular structures can be synthesized. The different morphologies of ZnO could be obtained using different amine sources, where different hydroxyl

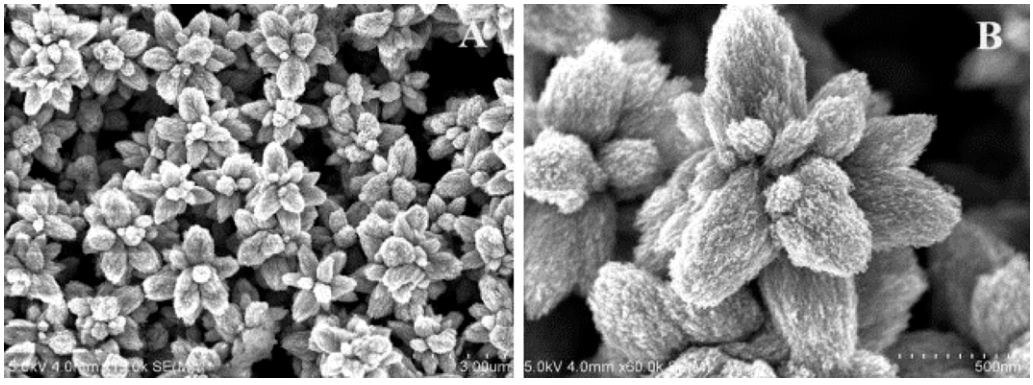

Fig. 6. SEM images of the prepared ZnO products. The scale bars of (A) and (B) represent 3 μm and 500 nm [47].

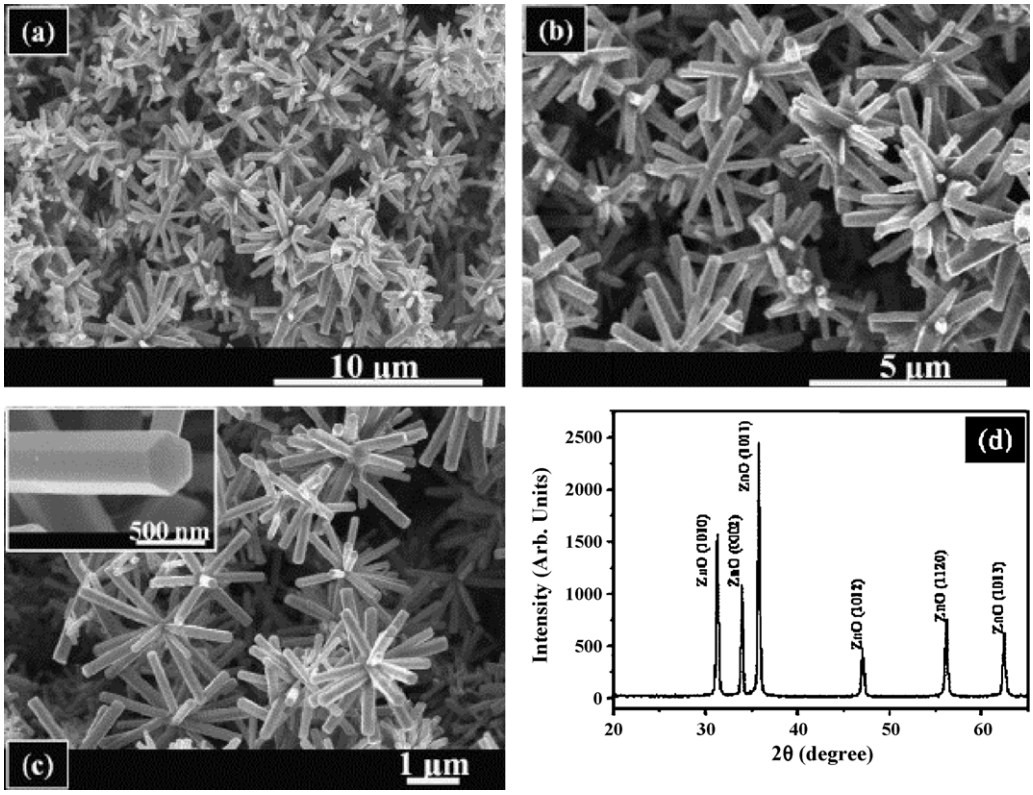

Fig. 7. (a–c) Typical FESEM images and (d) the X-ray diffraction pattern of grown flower-shaped ZnO structures composed of perfectly hexagonal-shaped ZnONRs [48].

ion releasing rates and their preferential adsorption contribute to different reaction rates and hence play a crucial role in controlling the assembly of different ZnO architectures [63–65]. Investigation related to the influence of parameters such as pH, concentration, time and growth temperature on the morphological control of ZnO nanostructures reveal that pH plays a crucial role in dictating the nano-morphologies [66]. Further, nanotetrapod-like, flower-like and urchin-like ZnO nanostructures can be obtained at higher pH values ($\geq$8), whereas rod-like structures can be obtained at lower pH values. Changes in concentrations result in changes in size and shape of nanostructures whereas, the growth temperature influence the aspect ratio of nanostructure [66]. The most common precursor used for ZnO nanostructure growth includes zinc nitrate ($Zn(NO_3)_2$) [25,67,68], zinc powder (Zn) [69], zinc chloride ($ZnCl_2$) [31,70], zinc acetate ($Zn(CH_3COO)_2$) [71–74] and zinc sulfate ($ZnSO_4$) [38,75], with growth-orienting reagents such as hexamethylenetetramine (HMTA) [25,30], ammonia (NH_3) [56], citric acid [35,76], ascorbic acid [47] and sodium hydroxide (NaOH) [71–73]. A great number of wet chemical/solution approaches have been documented in the last few years. Table 1 summarizes a number of such approaches used for the synthesis of ZnO nanostructures, many of which involve the deposition of a seed layer on a base matrix, which is subsequently utilized for nanostructure growth. A seed layer on base matrix from a seeding solution can be prepared by dipping [67,77,78], thermal decomposition [29], thermal evaporation [69], sputtering [23,79] or a sol–gel method [25]. Aluminum has also been reported as base matrix for ZnO nanostructure growth. During growth, base such as HMTA causes the

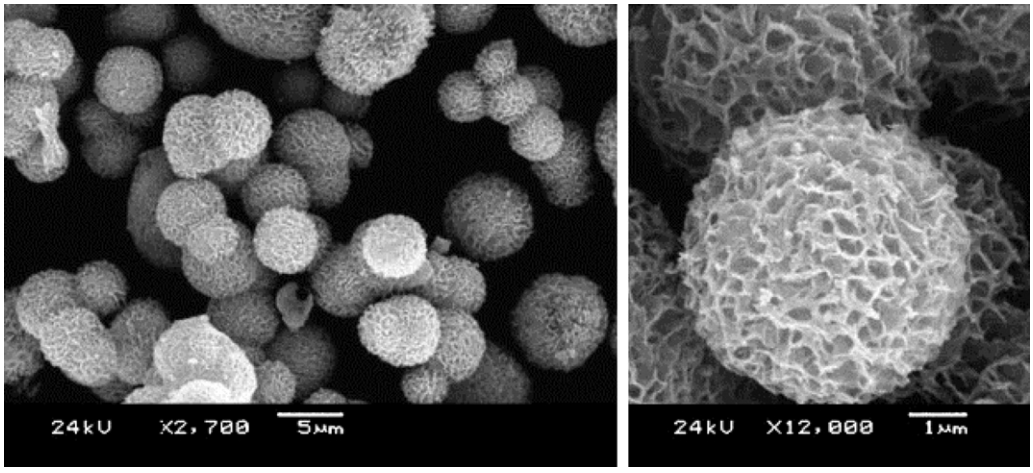

Fig. 8. SEM images of as-prepared porous nanosheet based ZnO microsphere with low (left) and high magnification (right) [50].

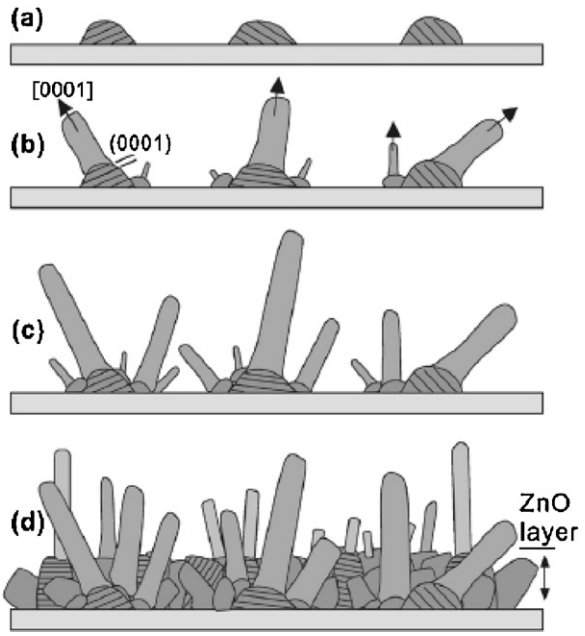

Fig. 9. Schematic illustration of the self-seeding VS growth mechanism of ZnONWs on a Si substrate [125].

formation of $Al(OH)_4^-$ on the surface of aluminum, which binds to the Zn^{2+}-terminated (001) surface and suppresses growth along the [001] direction, thus results in the lateral growth that forms oriented nanoflake ZnO [21,80].

In the formation of complex 3D ZnO nanostructures renucleation and sequential growth via Lamer-type nucleation-and-growth and Ostwald-ripening found to be the main reason. Further Al^{3+} ions were found to play important role in renucleation and the sequential growth process via (i) the precipitation of aluminium hydroxide ($Al(OH)_3$) to reduce OH^- concentration, thus supersaturating the growth solution and (ii) the absorption of $Al(OH)_3$ onto ZnO crystals that effects thermodynamic stability and the mass transfer process [81]. Recently ZnO nanostructure fabrication has also been reported using environment friendly sonochemical techniques [82,83]. Sonochemical technique provides a simple, mild, template-less and surfactant-free synthetic route [83]. Further, microemulsion based solvothermal methods have also been utilized in fabrication of flower-like and tube-like ZnO nanostructures [84].

2.2. Physical techniques

Physical techniques are the dry methods to obtain ZnO nanostructures. In these methods, one can obtain ZnO nanostructures with adequate control; however, these techniques typically require harsh temperature conditions. Most commonly employed physical techniques to grow ZnO nanostructures involve the carbothermal reduction process [124], thermal evaporation [24,27,125] vapor-phase transport method [32,37,126], etc.

Using a thermal evaporation method, Jong et al. described the initial growth of ZnONWs [125]. It was found that the growth process follows base growth mode, in which liquid droplet relics (a VLS mechanism) were not observed at the tip of the nanowires, whereas ZnO seeds were clearly observed at the bottom of the nanowires, suggesting that ZnO seeds formed, followed by growth of the nanowires on top of the seeds. Thus ZnONWs growth follow a self-seeding vapor–solid (VS) growth mechanism that occurred in four steps (Fig. 9): (1) formation of the ZnO seeds (hemispherical shape); (2) 1D epitaxial growth of the ZnONWs on the seeds by base

Table 2
Summary of various physical approaches for ZnO nanostructure synthesis.

Structure Type	Matrix	Technique	Growth reagent	Growth condition	Reference
ZnONW	Au coated Si	Carbothermal reduction	ZnO & graphite	900 °C, 30 min	[124]
ZnONW	Si	Thermal evaporation	ZnO & gold catalyst	Heating upto 900–950 °C followed by cooling	[27]
ZnONW	MWCNT/Si at 500 °C	Thermal evaporation	Zn	700 °C, 3 h	[24]
ZnONW	Si	Thermal evaporation	Zn	450 °C	[125]
ZnO nanotetrapods	Si	Vapor-phase transport	Zn & $Zn(CH_3COO)_2$	650 °C, 15 min	[37]
ZnONR	Si at 700 °C	Vapor-phase transport	ZnO & graphite	1100 °C, 30 min	[126]
ZnO nanocombs	Si	Vapor-phase transport	ZnO & graphite	900 °C, 30 min, 8×10^{-1} Torr	[32]
ZnO nanostructures	MWCNTs/PG	Vapor-phase self-catalysis	Zn, ZnO & graphite	750 °C, 15–30 min	[39,127]
ZnO nanotips	SiO_2, glass, c-sapphire	MOCVD	Diethylzinc, O_2	350–475 °C, 50 Torr	[6,128,129]
ZnONR	ZnO-Ga/SiO_2/Si	Low pressure CVD	Zn	600 °C, 30 min	[130]
Nanoporus ZnO film	Au coated glass	Rf magnetron sputtering	Zn	300 W, 50 mTorr	[55,131]
ZnO nanothin film	SiO_2	MOCVD	Diethylzinc, O_2	350 °C	[132]
ZnO nanothin film	Glass	Pulse laser deposition	ZnO	1.5–3 J cm^{-2} at 3×10^{-7} torr, KrF laser at 248 nm & 10 Hz	[133]
ZnO nanostructured thin film	Borosilicate glass	Rf magnetron sputtering	Zn	75 W, 1 Pa, 200 °C	[134]
ZnO nanotetrapods	Quartz plate	Thermal evaporation	Zn	900 °C	[135,136]
ZnONR	Au/Al_2O_3	VLS growth	ZnO & graphite	950 °C, 20–30 min, 300–400 mbar	[137]
ZnO nanoflakes & ZnONW	Glass	Localized oxidation	Zn film	300 °C, 5 min,	[138]
ZnO NW/belts	Sapphire	Thermal evaporation	ZnO	<1150 °C	[139]
Mn doped ZnO thin film	Si	Rf magnetron sputtering	ZnO	100 W, 2 Pa, room temperature	[140]

growth mode and the formation of additional seeds near existing seeds; (3) further acceleration of the 1D growth of the nanowires with continuous seeding; and (4) active formation of the ZnONWs with the formation of a ZnO layer on the Si substrate [125]. Table 2 shows the various procedure and condition used for synthesis of different ZnO nanostructures via physical methods.

2.3. Electrochemical methods

Recently, electrochemical techniques have gained much interest for growing ZnO nanostructures [22,44,46,51,141–144]. Electrochemical method allows the enhancement of nucleation density and the simple synthesis of doped ZnO nanostructures. Furthermore, in this method, many substrates do not require pre-treatment to generate a seed layer. The most common method for the electro-deposition of ZnO involves the reduction of oxygen or nitrate on the substrate in the presence of a Zn salt at neutral pH and elevated temperature. An increase in surface pH via generation of hydroxyl ions during reduction drives the formation of ZnO nanostructures in electrochemical methods. A decrease in pH at the surface lowers the solubility of ZnO at the surface by a factor of 1000, whereas the solubility in the bulk phase does not change, resulting in the deposition of ZnO nanostructures on the electrode surface [28]. Electrochemical procedure has been reported to synthesis ZnO and Pt-ZnO nanospheres (PtZnONS) onto GCE [22,46].

Electro-spinning is the other electrochemical technique for the synthesis of long, straight and aligned nanofibers [20,142]. Electro-spun fibers offer an attractive material of a sizable surface-to-volume ratio as a result of nanocrystalline structures and a relative simplicity in their positioning on a substrate [142]. Table 3 describes the various electrochemical approaches to grow ZnO nanodisks/sheets [51,52], ZnO nanoflowers [145], etc.

3. ZnO nanostructures and films as a matrix for biosensors

A matrix in a biosensor is a solid support used to provide a platform for the immobilization of a sensing molecule. The physical, chemical and surface properties of the desired support determine the method of immobilization and the operational stability of a biosensor. ZnO, which is a biomimetic semiconducting material, can be integrated with present day microelectromechanical systems (MEMS) and solid state technologies for the miniaturization of biosensors. Topoglidis et al. demonstrated the superior nature of ZnO as a matrix for the immobilization and bioelectrochemistry of proteins compared to titanium dioxide (TiO_2) [153]. The study demonstrated that ZnO films are more conductive at moderately applied potential, leading to electrochemical reduction of the immobilized protein at a lesser negative potential, which was further confirmed by spectroelectrochemical measurements. The high surface-to-volume ratio of ZnO nanostructures provides greater enzyme loading and provides a favorable microenvironment, which can preserve the activity of the immobilized biomolecules. In addition, because of their biocompatibility, ZnO nanostructures have been used in drug delivery. Tetrapod-like ZnO nanostructures have shown great promise in DNA purification, polymerase chain reaction and gene delivery [154]. Moreover, ZnO nanostructures, due to their excellent electron transfer rate, can evoke the hidden electrochemical ability of biomolecules. All enzymes possess redox capability, but this capability is not highlighted because the redox centers are insulated. ZnO based nanostructures can facilitate the direct electrochemistry of the enzymes [75,85].

ZnONP in composite form has provided a photoelectrochemical platform for biosensing [101]. In addition to nanostructures such as nanorods, nanocombs, nanotips, nanoflowers and nanowires, other ZnO nanostructures have been used for the immobilization

Table 3
Summary of various electrochemical approaches for ZnO nanostructure synthesis.

Structure Type	Matrix	Technique	Growth reagent	Growth condition	Reference
ZnO & Pt-ZnO nanosphere	GCE	Constant potential	$Zn(NO_3)_2$, HMTA, H_2PtCl_6	1 V, 1 h	[22]
ZnO nanofibers	Si	Electro-spinning	$Zn(CH_3COO)_2$ & PVP	Calcination	[20]
ZnO nanotubes	ITO	Electrochemical	$ZnCl_2$, KCl	(i) −1 V, 2000 s, (ii) 1.1 V, 1 h	[44,146]
ZnO nanotubes	Au	Chemical etching	$Zn(NO_3)_2$, HMTA, NaOH	(i) −0.8V, 85 °C, 7000 s, (ii) Etching at 85 °C, 90 min	[43]
ZnO nanodisks/sheets	ITO	Constant potential	$Zn(NO_3)_2$, KCl	(i) −0.9 V, 20 min, (ii) Sintering at 500 °C, 0.5–1.5 h	[51,52]
ZnO nanoflowers	MWCNT/GCE	Constant potential	$ZnCl_2$, KCl & H_2O_2	−1 V, 70 °C	[145]
Nanoporous ZnO film	MWCNT/GCE	Constant potential	$Zn(NO_3)_2$, KCl	−1.2 V, 30 min	[147,148]
Nanoporous ZnO film	Graphite	Constant potential	$Zn(NO_3)_2$ & SDS	−0.6 V, 5 min, 65 °C	[149]
Nanostructure ZnO film	ITO	Constant potential	$ZnCl_2$ & KCl	−1 to −1.4 V, 5–15 min, 70–80 °C	[150]
Nanostructure ZnO film	ITO	Constant potential	$Zn(NO_3)_2$, pH 5	−2.5 V, 10 min, 65 °C	[54]
Nanostructure ZnO film	Au	Cyclic voltammetry	$Zn(NO_3)_2$, KCl	−1 to 1 V, 2 scan, 70 °C	[151]
ZnO nanobelt	ITO or conducting PET	Constant potential	$Zn(NO_3)_2$, KCl	−1.4 V, 0 °C	[46]
ZnONR	Transparent conductive oxides coated glass	Electrochemical	$Zn(NO_3)_2$,	30 min, 80 °C	[152]
ZnO nanopillar array and ZnONW	Nanoporus polycarbonate membrane template and Au/Si	Constant current	$ZnCl_2$, KCl & H_2O_2	−0.1 mA, 30 min	[143,144]
Zno nanofibers	SiO_2/Si	Electro-spinning	$Zn(CH_3COO)_2$ & Poly (vinyl alcohol)	(i) 10 kV, 0.1 mL h^{-1}, 22 °C (ii) Calcinations at 500 and 700 °C, 4 h	[142]

of proteins. Nanoporous structures have been investigated to highlight the importance of the microenvironment and electron transfer properties that are provided by nanomaterials. The conformational changes in the enzyme upon immobilization on nanosurfaces contribute to alter the affinity of the enzyme toward its substrate and is accessed by calculating Michaelis-Menten constant (K_m), compared to that of the free enzyme [85]. Saha et al. investigated the influence of surface defects (interstitial Zn and antisite oxygen) in radio frequency (rf) magnetron sputtered nanoporous ZnO film on its biosensing response properties. The study revealed the correlation between biosensing properties and the presence of defects. Films deposited under high pressure (50 mT) were found to be more sensitive and were attributed for the availability of more surface area for effective immobilization of the biomolecule and the suitable microenvironment with the high-quality electron transfer characteristics of the nanoporous ZnO thin film [131].

3.1. Immobilization of biomolecules on ZnO based matrices

The stability of the biosensing molecule on the matrix surface strongly depends on the immobilization and surface chemistry. Various immobilization techniques have been employed to immobilize biosensing molecules on a ZnO based matrix. Among them, physical immobilization and cross-linking has predominantly been used [21,27,37,155–157]. The high isoelectric point (approximately 9) of ZnO facilitates the physical immobilization of biomolecules such as glucose oxidase (GOx), cholesterol oxidase (ChOx), tyrosinase, uricase, myoglobin, biotin and microperoxidase on a ZnO surface [21,22,37,40,72,149,158,159]. At neutral pH, ZnO possesses a positive charge, whereas enzymes with low IEPs behave like a negative charged species, which leads to an electrostatic interaction between them and result in their physical binding. Armelao et al. proposed a novel approach to synthesize DNA microarrays by immobilizing the nucleic acid on ZnO surfaces using the phosphate backbone of the DNA. The optimized film showed a high density of binding sites, making it a promising candidate for DNA microarray fabrication. The scanning of the dye-labeled DNA printed onto the oxide layer revealed the presence of regular-shaped spots, indicating efficient anchoring of the DNA on the oxide platform [160]. The ZnO matrix was reported to provide an advantageous microenvironment in terms of activity retention [72].

Chemical binding and Nafion-assisted cross-linking technique has also been successfully employed to immobilize biomolecules on ZnO based matrix [157,161,162]. Corso et al. studied antibody immobilization methods on ZnO surfaces for biosensor applications and showed that modifying ZnO surface by silane chemistry results in enhanced binding and sensing efficiency [163].

4. ZnO nanostructure based biosensors

ZnO based matrices have been used for the binding of various biosensing molecules, such as GOx, ChOx, uricase, horseradish peroxidase (HRP), microperoxidase and tyrosinase, for the detection of their respective analytes in various device configurations [164–168]. Further, various biomolecules such as ssDNA, antibodies, antigens and other proteins like myoglobin, hemoglobin (Hb), etc. have been used for immobilization onto ZnO surfaces for biosensor applications [50,149,160,169,170]. ZnO based biosensors have been developed in various configurations with field effect transistors (FET), ion-sensitive field effect transistors (ISFET), optical devices, piezoelectric devices and electrochemical transducers. Piezoelectric devices using ZnO as material for biosensing applications include SAW, quartz crystal microbalance (QCM), film bulk acoustic resonator (FBAR) or flexural plate wave (FPW). ZnO films for acoustic wave based sensing and applications have been reviewed by Fu et al. [8]. For ZnO nanostructure based matrix, an electrochemical transduction has been most utilized. Recently, a few studies have also been conducted on optical transduction and on FETs by modifying FETs with proteins for biosensing. FETs as ISFET for sensing can undergo miniaturization on microchips with a capability of multi-analyte sensing. The potential shown by these studies suggests that FETs will replace electrochemical detection as the choice for miniaturized biosensor applications. Recently, Ali et al. demonstrated a ZnONW array based, wireless remote monitoring of glucose using an existing general packet radio services (GPRS)/global system for mobile communication (GSM) network. Similar techniques with various ZnO nanostructure based platforms in the future can provide nanosensor/nanodevices for monitoring multiple health parameters outside central labs [61].

4.1. Biosensors based on electrochemical transduction

Electrochemical techniques have been the most widely used form of transduction in biosensing applications. These transducers sense a biochemical signal generated by a bio-receptor (e.g., enzyme) via an electrochemical pathway such as amperometric, potentiometric or conductometric. Among electrochemical techniques, the cyclic voltammetry (CV), differential pulse voltammetry (DPV) and amperometric techniques are most commonly used for biosensing applications. A large number of publications have appeared in last five years on amperometric biosensors based on ZnO as the immobilization matrix [171]. In electrochemical biosensors electron transfer between redox-active biomolecules to electrodes is essential [172]; however, electron transfer does not always occur directly but rather occurs through the use of redox mediators. In biosensors based on direct electron transfer (DET), the absence of mediators is the primary advantage, providing the sensor with superior selectivity because both the electrode material and the enzyme operate in a potential window closer to the redox potential of the enzyme itself. Therefore, the sensor is less prone to interfering reactions. Direct and mediated electron transfer between proteins and electrodes has been extensively studied and well-reviewed [173–180].

DET between the electrode material and redox-active biomolecules has been understood since 1977 and reported for number of proteins and enzymes. In principle, two experimental approaches are used to establish DET between redox enzymes and electrodes: (i) indirect evidence obtained by observing a catalytic response current in the presence of the enzyme substrate (ii) direct evidence from the observation of independent electrochemical activity of the redox cofactor comprising the active site in the absence of substrate [173–176]. Recently, nanostructured electrodes that have been fabricated using carbon nanomaterials, Au nanoparticles and metal oxides have been adopted as a promising method to facilitate the DET of proteins [181,182]. Among nanomaterials, ZnO nanostructures are attracting increasing interest for DET based biosensors [49,183–185]. Deng et al. described DET in zinc–superoxide dismutase (Zn–SOD) system and showed that SOD is stable when immobilized on the nanostructured ZnO film and processes its intrinsic enzymatic activity after getting adsorbed on ZnO nanoparticles [185]. The interaction studies on GOx immobilized onto tetragonal pyramid-shaped porous ZnO (TPSP-ZnO) nanostructures via AFM, N_2 adsorption isotherms and electrochemical methods has shown direct electrochemical behavior of matrix [75]. Fatemi et al. demonstrated a biomorphic porous ZnO nanostructure based direct electrochemical biosensor. The biomorphic porous ZnO nanostructures were effective in facilitating the electron transfer of the immobilized component due to the unique morphology and smaller-than-average crystallite size. A reagent-less uric acid biosensor based on ZnONRs by Zhang et al. [158] demonstrated the electro-catalytic activity of ZnO to

Table 4
Characteristics of various electrochemical transduction based biosensors using a ZnO nanostructure matrix.

ZnO nanostructure	Biomolecule	Analyte	Response characteristics	Reference
ZnONR	Uricase	Uric acid	[L]: 5.0×10^{-6} to 1.0×10^{-3} mol L^{-1}; [DL]: 2.0×10^{-6} mol L^{-1}; [K_m]: 0.238 mM	[158]
ZnO nanocomb	GOx	Glucose	[S]: 15.33 μA cm^{-2} mM^{-1}; [K_m]: 2.19 mM, [DL]: 0.02 mM	[32]
ZnONR	GOx	Glucose	[S]: 23.1 μA cm^{-2} mM^{-1}; [RT]: 5 s; [L]: 0.01–3.45 mM; [DL]: 0.01 mM; [K_m]: 2.9 mM	[70]
ZnO-Co nanocluster	GOx	Glucose	[S]: 13.3 μA cm^{-2} mM^{-1}; [DL]: 20 μM; [K_m]: 21 mM	[162]
ZnONW	GOx	Glucose	[RT]: 5 s; [L]: 0.01–1.6 mM; [S]: 35.3 μA cm^{-2} mM^{-1}; [DL]: 1 μM; [K_m]: 1.54 mM	[85]
Tetragonal pyramidal ZnO nanostructure	GOx	Glucose	[L]: 0.05–8.2 mM; [DL]: 0.01 mM	[75]
Nanoporous ZnO thin film	ChOx	Cholesterol	[L]: 25–400 mg dL^{-1}; [K_m]: 2.1 mM; [SL]: 10 weeks	[55]
ZnONP	ChOx	Cholesterol	[L]: 5–300 mg dL^{-1}; [DL]: 5 mg dL^{-1}; [S]: 1.41×10^{-4} A mg dL^{-1}; [K_m]: 8.63 mg dL^{-1}; [RT]: 15 s; [SL]: 85 days	[186]
ZnO nanoflowers	ChOx	Cholesterol	[S]: 61.7 μA mM^{-1} cm^{-2}; [RT]: 5 s; [DL]: 0.012 μM; [L]: 1.0–15.0 μM; [K_m]: 2.57 mM	[48]
ZnONP	ChOx	Cholesterol	[S]: 23.7 μA mM^{-1} cm^{-2}; [DL]: 0.37 ± 0.02 nM; [RT]: 5 s; [L]: 1.0–500.0 nM; [K_m]: 4.7 mM	[86]
ZnO nanoflower	HRP	H_2O_2	[L]: 1.5×10^{-5} to 1.1×10^{-3} M; [DL]: 9.0×10^{-6} M	[49]
ZnO nanoflower	HRP-labeled nanogold	H_2O_2	[L]: 1.5×10^{-6} to 4.5×10^{-4} M; [DL]: 7.0×10^{-7} M; [S]: 369 μA mM^{-1} cm^{-2}	[73]
ZnO nanoflower	HRP	H_2O_2	[RT]: 5 s; [L]: 1.0×10^{-5} to 1.8×10^{-3} M; [DL]: 2.0 μM; [SL]: 40 days	[71]
nanoporous ZnO	HRP	H_2O_2	[RT]: 10 s; [L]: 5.0×10^{-6} to 2.0×10^{-3} mol L^{-1}; [S]: 43.8 μA L $mmol^{-1}$	[187]
nanoporous ZnO film	Myoglobin	H_2O_2	[L]: 4.8×10^{-6} to 2.0×10^{-4} mol L^{-1}; [DL]: 2.0×10^{-6} mol L^{-1}	[149]
ZnONPs	Microperoxidase	H_2O_2	[L]: 1×10^{-7} to 8×10^{-4} mol L^{-1}; [DL]: 3×10^{-8} mol L^{-1}; [S]: 0.041 μA μM^{-1}	[40]
ZnO nanosheet based microsphere	Hemoglobin	H_2O_2	[L]: 1–410 μM; [K_m]: of 143 μM; [SL]: 20 days	[50]
ZnONPs	Hemoglobin	H_2O_2	[K_m]: 0.075 mmol L^{-1}; [RT]: 4 s; [L]: 1.94×10^{-7} to 1.73×10^{-3} mol L^{-1}; [DL]: 9.7×10^{-8} mol L^{-1}	[88]
ZnONR		Hb and cytochrome c (cyt-c).	HB: [L]: 5×10^{-7} to 2×10^{-5} mol L^{-1}; [DL]: 2×10^{-7} mol L^{-1} Cyt-c: [L]: 5×10^{-7} to 3×10^{-5} mol L^{-1}; [DL]: 3×10^{-7} mol L^{-1}	[188]
ZnONR	Tyrosinase	Phenol, catechol	Phenol: [L]: 0.02 to 0.1 mM; [K_m]: 0.24 mM; [S]: 0.83 μA mM^{-1} Catechol: [L]: 0.01 to 0.4 mM; [K_m]: 1.75 mM; [S]: 2.14 μA mM^{-1}	[126]
ZnONP	Tyrosinase	Phenol, catechol	p-Cresol: [S]: 187 μA $mmol^{-1}$ L; [DL]: 5.0×10^{-9} mol L^{-1}; [L]: 1.0×10^{-8} to 7.5×10^{-5} mol L^{-1}; [K_m]: 21 μmol L^{-1} Phenol [S]: 182 μA $mmol^{-1}$ L; [DL]: 5.0×10^{-8} mol L^{-1}; [L]: 1.5×10^{-7} to 6.5×10^{-5} mol L^{-1}; [K_m]: 23 μmol L^{-1} Catechol [S]: 114 μA $mmol^{-1}$ L; [DL]: 3.0×10^{-8} mol L^{-1}; [L]: 1.0×10^{-7} to 7.5×10^{-5} mol L^{-1}; [K_m]: 40 μmol L^{-1}	[72]
ZnONPs	ss DNA	DNA (PAT gene)	[DR]: 1.0×10^{-11} to 1.0×10^{-6} mol L^{-1}; [DL]: 2.8×10^{-12} mol L^{-1}	[87]
ZnONPs	ssDNA	DNA (PAT gene)	[DL]: 2.8×10^{-12} mol L^{-1}; [L]: 1.0×10^{-11} to 1.0×10^{-6} mol L^{-1}	[189]
Nanoporous ZnO	IgG antibody	Human IgG	[DR]: 2.5–500 ng mL^{-1}; [DL]: 1.2 ng mL^{-1}	[190]
ZnO nanofork	HRP	H_2O_2	[L]: 5×10^{-5} M to 7×10^{-4} M; [DL]: 0.3 μm; [S]: 201.12 μA mM^{-1}; [RT]: 3 s; [K_m]: 0.292 mM	[33]

Table 4 (*Continued*)

ZnO nanostructure	Biomolecule	Analyte	Response characteristics	Reference
Waxberry ZnO microstructure	HRP	H_2O_2	[L]: 1.5×10^{-4} to 15 mM; [DL]: 1.15×10^{-4} mM	[34]
ZnONF	GOx	Glucose	[S]: 70.2 μA cm^{-2} mM^{-1}; [RT]: 4 s; [L]: 0.25–19 mM; [DL]: 1 μM; [SL]: 4 months	[20]
ZnO nanobundles	GOx	Glucose	[L]: 0.01–0.25 mM; [DL]: 0.01 mM	[35]
ZnO tetrapod	GOx	Glucose	[S]: 25.3 μA mM^{-1} cm^{-2}; [DL]: 4 μM; [K_m]: 5.05 mM; [RT]: 6 s; [L]: 0.005–6.5 mM	[37]
ZnONTs	GOx	Glucose	[L]: 50 μM–12 mM; [S]: 21.7 μA mM^{-1} cm^{-2}; [DL]: 1 μM; [K_m]: 19 mM	[43]
ZnONT	GOx	Glucose	[S]: 30.85 μA cm^{-2} mM^{-1}; [L]: 10 μM–4.2 mM; [DL]: 10 μM; [K_m]: 2.59 mM	[44]
ZnONPs	GOx	Glucose	[L]: 0.1–16 mM; [S]: 50.2 mA cm^{-2} M^{-1}; [DL]: 250 nM; [SL]: 160 days	[39]
ZnONPs	GOx	Glucose	[DL]: 5.6×10^{-6} M under illumination and 1.1×10^{-4} M in the dark	[89]
Nanostructured ZnO film	ChOx	Cholesterol	[L]: 5–400 mg dL^{-1}; [DL]: 0.5 mg dL^{-1}; [RT]: 10 s; [S]: 0.059 μA (mg dL^{-1} cm^{-2})$^{-1}$; [K_m]: 0.98 mg dL^{-1}	[53]
Nanostructured ZnO film	Urease and glutamate dehydrogenase	Urea	[L]: 10–80 mg dL^{-1}; [DL]: 13.5 mg dL^{-1}; [K_m]: 6.1 mg dL^{-1}	[54]
Nanostructured ZnO film	DNA probes specific to *M. tuberculosis*	Complementary target and genomic DNA	[DL]: 1×10^{-12} M for a complementary target and 1×10^{-13} M for genomic DNA; [RT]: 60 s; [SL]: 4 months; [L]: 1×10^{-6} to 1×10^{-12} M; [Re]: 10 times	[150]
Pt-ZnO nanospheres	ChOx	Cholesterol	[L]: 0.5–15 μM; [S]: 1886.4 mA M^{-1} cm^{-2}; [RT]: 5 s; [SL]: 5 weeks	[22]
ZnO nanoflakes	GOx	Glucose	[L]: 500 nM–10 mM; [RT]: 4 s; [S]: −65.2 mV $decade^{-1}$	[21]
Hexagonal ZnO nanosheets	Cyt-c	H_2O_2	[S]: 2.0 ± 0.1 μA cm^{-2} mM^{-1}; [DL]: 0.8 μM; [L]: 1–1000 μM	[51]
ZnO nanocombs, nanorods and hierarchical nanodisks	GOx	Glucose	ZnO nanocomb: [DL]: 20 μmol L^{-1}; [RT]: 10 s; [S]: 15.33 μA cm^{-2} (mmol L^{-1})$^{-1}$; [K_m]: 2.19 mmol L^{-1} ZnONRs: [DL]: 10 μmol L^{-1}; [RT]: 5 s; [S]: 23.1 μA cm^{-2} (mmol L^{-1})$^{-1}$; [K_m]: 2.9 mmol L^{-1} ZnO hierarchial nanodisks: [DL]: 10 μmol L^{-1}; [RT]: 10 s; [S]: 16.9 μA cm^{-2} (mmol L^{-1})$^{-1}$; [K_m]: 2.61 mmol L^{-1}	[31]
ZnONW	GOx	Glucose	[L]: 1×10^{-4} to 1×10^{-2} M	[27]
Porous ZnO nanofilm		Hydroxylamine	[L]: 0.4–1.9×10^4 μM; [DL]: 0.12 μM; [RT]: 3 s; [S]: 0.0075 μA μM^{-1}	[147]
ZnO nanoflower and nanobelt	Urease	Urea	[L]: up to 50 mM; [RT]: 6 s; Nanobelt structure of ZnO resulted in highest urea sensitivity.	[45]
ZnONW	GOx	Glucose	[L]: 0.5 μM–10 mM; [RT]: 4 s; [S]: 35 mV $decade^{-1}$	[78]
ZnONR	GOx	Glucose	[L]: 0.5–1000 μM; [RT]: 1 s	[191]
ZnONW	DNA	Sequence-specific target DNA	[L]: 1×10^{-13}–1×10^{-7} M; [DL]: 3.5×10^{-14} M and selectivity for single-mismatched DNA.	[124]
ZnONR	GOx	Glucose	[L]: 5–300 μM; [DL]: 3 μM; [RT]: 5 s	[29]
Hexagonal ZnONRs	ChOx	Cholesterol	[L]: 1×10^{-6} to 1×10^{-2} M; [S]: 35.2 mV $decade^{-1}$; [RT]: 10 s	[67]
Rod-constructed ZnO microspheres	Myoglobin	H_2O_2	[L]: 2–490 μM; [DL]: 0.21 μM; [K_m]: 32 μM	[42]

Table 4 (*Continued*)

ZnO nanostructure	Biomolecule	Analyte	Response characteristics	Reference
ZnONRs	GOx	Glucose	[L]: 0.1–33.0 μM; [DL] 10 nM; [RT]: 5 s, [K_m]: 0.41 mM; [S]: 1492 μA mM^{-1} cm^{-2}	[156]
ZnONR	Tyrosinase	Phenolic compounds	*p*-cresol: [L]: 1–210 mM; [S]: 179.9 μA mM^{-1} cm^{-2} Phenol: [L] 1–190 mM; [S]: 90.2 μA mM^{-1} cm^{-2} 4-chlorophenol: [L] 1–250 mM; [S]: 121.3 μA mM^{-1} cm^{-2}	[155]
ZnONR microarrays	Tyrosinase	Phenolic compounds	*p*-cresol: [L]: 1–175 μM; [DL] 0.1 μM; [S]: 576.2 μA mM^{-1} cm^{-2} 4-chlorophenol: [L] 1–150 μM; [DL] 0.25 μM; [S]: 339.3 μA mM^{-1} cm^{-2} Phenol: [L] 1–150 μM; [DL] 0.2 μM; [S]: 287.1 μA mM^{-1} cm^{-2}	[192]
ZnO nano tetragonal pyramid	HRP	H_2O_2	[RT]: 10 s; [L]: 0.4–260 mM	[38]
ZnO QDs	Anti-CA 19-9	Carbohydrate antigen (CA) 19-9	[L]: 0.1–180 U mL^{-1}; [DL]: 0.04 U mL^{-1}	[26]
ZnONP	Enzyme free	Glucose	[L]: 5×10^{-13} to 2×10^{-8} mol;	[193]
ZnONR	GOx	Glucose	[L]: 0.128–8 mM; [S]: 160.8 mV $decade^{-1}$	[95]
ZnO solgel	Tyrosinase	Phenol	[L]: 0.06–32 μM; [DL]: 0.047 μM; [RT]: 2 s; [S]: 0.77 A M^{-1}; [K_m]: 18 μM	[194]
ZnO nanowalls	ChOx	Cholesterol	[L]: 1×10^{-6} to 1×10^{-3} M; [RT]: 5 s; [S]: 53 mV $decade^{-1}$	[100]
ZnONP	Porphyrin	Cysteine	[L]: 0.6–157 μmol L^{-1}; [DL]: 0.2 μmol L^{-1}; [RT]: 3 s	[101]
ZnONP	Xanthine oxidase	Xanthine	[L]: 0.8–40 μM; [DL]: 0.8 μM; [RT]: 5 s; [SL]: 100 days; [K_m]: 13.51 μM	[99]
ZnO nanotetrapods	GOx	Glucose	[DL]: 0.5 mM	[195]
ZnONR	Antibody	E. coli	[L]: 10^2–10^6 cfu mL^{-1}; [DL]: 50 cfu mL^{-1}	[196]
ZnONP	Creatinine amidohydrolase, creatine amidohydrolase and sarcosine oxidase	Creatinine	[L]: 10–650 μM; [DL]: 0.5 μM; [RT]: 10 s; [S]: 0.03 μA μM^{-1} cm^{-2}; [SL]: 120 days; [K_m]: 0.35 mM	[98]
ZnONP	ssDNA	Trichoderma harzianum	[L]: 1×10^{-14} to 1.8×10^{-4} mol L^{-1}; [DL]: 1×10^{-15} mol L^{-1}	[197]
ZnONP	L-lactate oxidase	L-lactate	[L]: 0.2–2 mM; [DL]: 6 μM; [RT]: 6 s; [S]: 7.3 μA mM^{-1}; [SL]: 120 days; [K_m]: 1.5 mM	[127]
ZnONP	GOx	Glucose	[L]: 6.67 μM–1.29 mM; [DL]: 2.22 μM; [S]: 10.03 μA mM^{-1} cm^{-2}; [K_m]: 2.48 mM	[148]
ZnONP	Lapase, glycerol kinase and glycerol-3-phosphate oxidase	Triglyceride	[L]: 50–650 mg dL^{-1}; [DL]: 20 mg dL^{-1}; [RT]: 6 s; [SL]: 7 month	[97]
ZnONT	GOx	Glucose	[L]: 5×10^{-6} to 12×10^{-3} M; [RT]: 4 s; [S]: 69.12 mV $decade^{-1}$	[96]
Nanostructured ZnO film	GOx	Glucose	[L]: 1.38–22.22 mM; [DL]: 0.05 mM; [S]: 1.27 μA mM^{-1} cm^{-2}; [SL]: 11 weeks; [K_m]: 1.11 mM	[131]
ZnO nanosphere	Haemoglobin	H_2O_2	[L]: 1.8 μM–2.3 mM; [DL]: 0.6 μM; [K_m]: 1.46 mM	[198]
ZnO QD	Concanavalin-A	Allergy chicken ovomucoid	[L]: 1–140 ng mL^{-1}; [DL]: 1 ng mL^{-1}	[90]
ZnO hollow nanosphere	GOx	Glucose	[L]: 0.005–13.15 mM; [DL]: 1 μM; [S]: 65.82 μA mM^{-1} cm^{-2}	[82]
ZnONR	Hemoglobin	H_2O_2	[L]: 0.01–3.2 μM; [DL]: 0.009 μM; [K_m]: 0.0019 μM	[123]
Porous ZnO nanostructure	GOx	Glucose	[L]: 0.01–1 mM; [DL]: 10 μM; [S]: 23.4 μA mM^{-1} cm^{-2}; [RT]: 7 s	[184]

Sensitivity [S], Linearity [L], Detection limit [DL], Detection range [DR], Michaelis-Menten constant [K_m], Response time [RT], Shelf life [SL] and Reusability [Re].

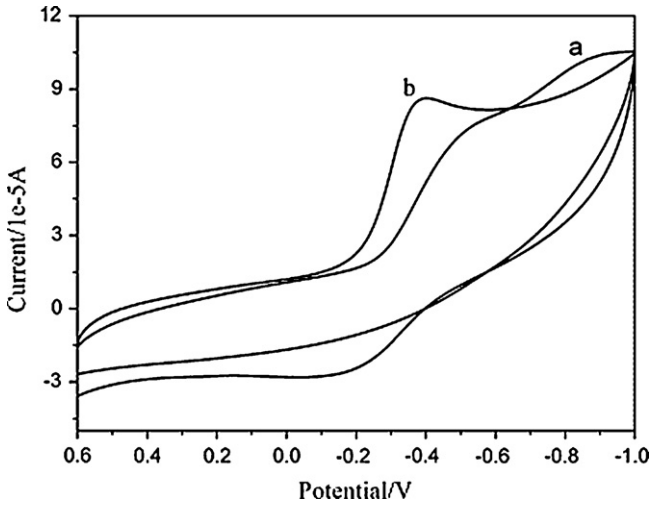

Fig. 10. Cyclic voltammograms of (a) Hb–PVA/GCE, (b) Hb–ZnO–NRs/PVA/GCE in phosphate buffer (pH 7.0). Scan rate: 100 mV s^{-1} [123].

the oxidation of uric acid without requiring an electron mediator. Observed low K_m value indicated high affinity of bound urease toward uric acid. In addition to DET, excellent thermal stability and anti-interference ability were attributed to the conducting ZnONR matrix [158]. Using enhanced DET between the enzyme active site and the electrode, a ZnO nanocomb based biosensor was reported by Wang et al. for glucose detection [32]. DET provided by the nanoscale transport channel of the single crystalline ZnO nanostructures resulted in high sensitivity without an electron mediator [32].

A flower-like ZnO-AuNP-nafion nanocomposite film prepared through a wet-chemical route was found to promote DET from the immobilized HRP. The combined use of flower-structured ZnO and AuNPs resulted in the enhanced ability of the electrode to reduce H_2O_2 electro-catalytically. Further, higher affinity of the immobilized enzyme toward H_2O_2 was suggested by a low value of K_m (1.76 mM) and was attributed to the positive conformational changes in the enzyme that were caused by the suitable microenvironment provided by the nanostructured ZnO matrix [49]. In another study, Liu et al. described ZnO in flower-shaped nanostructures dispersed in a CHIT based matrix for HRP immobilization. The enzyme immobilized ZnO-CHIT composite bioelectrode showed short response time and attributed to the rapid reduction of H_2O_2 due to the porous structure, which provides a low mass transport barrier and results in the rapid diffusion of the substrate from the electrolyte solution to ZnO that provides a good path for charge carriers [71]. In addition, DET reactions of microperoxidase were achieved by ZnONPs and further enhanced by UV irradiation. The experimental data clearly showed that the ZnONPs facilitated the electron transfer, which activated the redox reaction by the microperoxidase enzyme. The enhanced catalytic ability of the microperoxidase by UV was attributed to an improvement in conduction due to the ZnONPs, which are known to exhibit photocatalytic activity. This electrochemical activity of the microperoxidase was exploited toward the reduction of H_2O_2, leading to a H_2O_2 biosensor [40]. In poly(vinyl alcohol) (PVA)/ZnONRs composite film based H_2O_2 biosensor, ZnONRs provided a suitable microenvironment for Hb immobilization. Compared with the Hb–PVA electrode, Hb–ZnONRs/PVA electrode exhibited a greater response, which was attributed to the ZnONRs facilitating the electron transfer between the Hb and the GCE (Fig. 10) [123]. Thus, a matrix based on a PVA/ZnONRs film can provide an attractive surface for the immobilization of biomolecules due to its good biocompatibility, negligible swelling in aqueous solutions and the

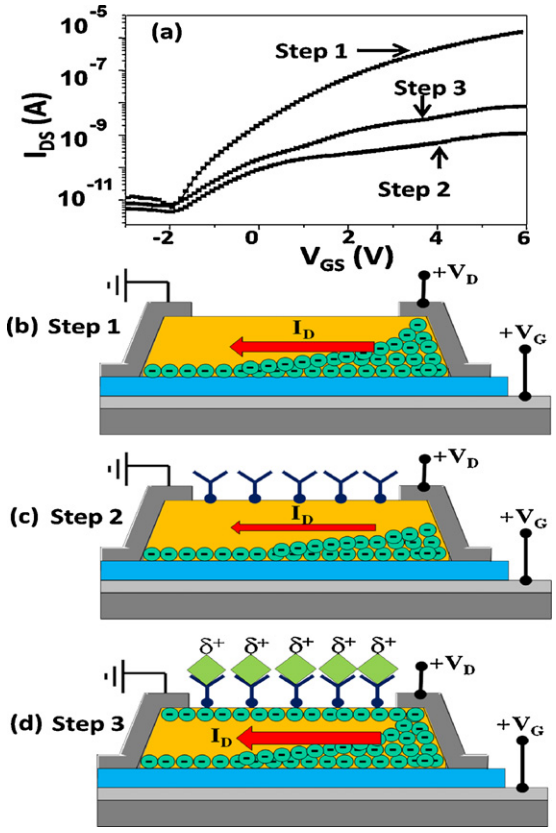

Fig. 11. (a) Drain current versus gate bias for a fixed drain bias of 10 V. Step 1: bare device; Step 2: EGFR-antibody immobilization; and Step 3: EGFR protein detection. [(b)–(d)] Schematic of the carrier modulation mechanism for steps 1–3, respectively [132].

presence of large amount of hydrogen bonds in the composite film to maintain the configuration of the biomolecule [123]. Table 4 summarizes the various ZnO nanostructure matrix based electrochemical biosensors.

4.2. Biosensors based on optical transduction and field effect transistors

In addition to the methods described above, optical and FET (Fig. 11) [132], based detection of biomolecules has been used on ZnO matrices. These techniques have demonstrated their applications in gene profiling, enzyme-linked immunosorbent assay, cellular imaging, proteomics, disease diagnosis and environmental analysis. Dorfman et al. reported the development and utilization of a nanoscaled ZnO platform to enhance the fluorescence detection of biomolecules such as DNA and proteins [199]. Strong fluorescence emission was observed from a ZnO platform immobilized with fluorescein conjugated antibovine IgG (FITC-IgG), which allowed for attomolar detection. A direct comparison of the fluorescence signal observed in size-comparable ZnONRs and Si nanorods showed a much stronger fluorescence emission by the ZnO system over the Si system and this boost was attributed to the inherent properties of ZnO. Although the fluorescence was weaker in ZnO thin films compared to ZnONRs, the emission was still stronger than that of other planar materials, making it an attractive alternative. The fluorescence emission using this platform was three orders of magnitude higher than that using Si, Si nanorods, glass, quartz and polymethylmethacrylate platforms. Enhanced fluorescence emission in the presence of ZnONRs was explained by changes in the photonic mode density and a reduction in the self-quenching of fluorophores. The presence of ZnONRs was considered to bring

out modifications in the decay rates of radiative and nonradiative pathways, leading to a dominantly rapid radiative decay. The ZnO nanoplatform permitted successful fluorescence detection of fluorophore-labeled DNA molecules at DNA concentrations as low as tens of attomolar when detecting with a mercury arc lamp and a few nanomolar range when using an Ar laser [199].

Hong et al. described immunoassays using bifunctional Fe_3O_4/ZnO/Au nanorices as Raman probes. The authors demonstrated that the superparamagnetic property of the nanorices leads to their separation and purification, whereas unsusceptible multiphonon resonant Raman scattering of the nanorices provides a characteristic spectroscopic fingerprint function for the accurate detection of the analyte. Furthermore, the presence of Au improved the water solubility of ZnO and facilitated the conjugation of biomolecules [92]. Park et al. described a biosensor for the protective antigen (PA 83) of anthrax. Using an FITC-labeled PA affinity peptide-modified ZnONRs array, a detection limit of 150 aM was achieved for PA 83. However, in the absence of nanorods, the fluorescence signal of the PA-peptide complex reduces significantly, suggesting the inhibition of the self-quenching properties of the fluorophore by ZnONRs [3].

ZnO-Au nanocomposites have been used for the fabrication of a surface plasmon resonance based biosensor for rabbit IgG detection. The strong localized electromagnetic field generated in ZnO-Au nanocomposite at resonance condition resulted in 16-fold improvement in detection limit [36]. Utilizing SPR-induced electron transfer between Au and ZnO at resonance conditions, Singh et al., demonstrated the SPR based glucose biosensor and achieved enhanced sensitivity, which was attributed to SPR-induced electron transfer and the presence of a large number of defects and trapped oxygen ions on electrochemically deposited ZnO film surface, that contribute extra electrons to the active layer [151]. Table 5 shows the characteristics of various optical and FET transduction based biosensors using a ZnO nanostructure matrix.

4.3. Biosensors based on piezoelectric transduction

Recently, researchers have shown interest in piezoelectric properties of ZnO for biosensing. Piezoelectric devices are sensitive to mass loading and are often termed gravimetric devices [204]. With the application of an alternating voltage, piezoelectric crystal oscillates in a thickness shear mode with the faces of the crystal vibrating in opposite directions gives rise to a resonant frequency response that can be modulated by change in mass on the crystal surface and can be used for sensing. Piezoelectric biosensors are mainly based on QCM and Surface acoustic wave principles. In piezoelectric transduction, SAW sensors utilize a surface wave effect instead of a bulk acoustic wave effect in QCM and dominate in sensitivity. Zhang et al. reported a ZnO nanotip based QCM sensor to detect the loading of DNA oligonucleotides. The results suggested that a ZnO nanotip surface provides a large surface area for binding and thus causes a 10 times larger frequency shift on immobilization of the DNA than that of a regular QCM sensor. Further, the super hydrophilicity of ZnO nanotips exhibited under UV illumination allows for the detection of analytes that could not be detected by traditional QCMs [205]. Reyes et al. also showed that a super hydrophilic ZnO nanotip layer increases the mass loading frequency shift of the device tenfold compared to a standard QCM. Furthermore, the nanotip layer also significantly reduces the sample volume [129]. Lee et al. studied ZnONR-modified quartz crystals as a liquid-phase sensor and showed that the device can be used as a DNA biosensor. The nanorod-modified QCM exhibited sensitivity to the immobilization of thiolated oligonucleotides and to hybridization [79].

Surface acoustic wave based biosensors are a branch of acoustic devices that involve transduction from electric energy to

Table 5
Characteristics of various optical and FET transduction based biosensors using a ZnO nanostructure matrix.

ZnO nanostructure	Biomolecule	Analyte	Transducer	Response characteristics	Reference
ZnONRs	PA affinity peptide	Protective antigen (PA 83)	Fluorescence	[L]: 15 aM–1.5 nM; [DL]: 150 aM	[3]
ZnO/SiO_2 (core/shell) nanorod arrays	Oligonucleotide probes	DNA	Fluorescence	Nanorod arrays not only enhances the fluorescence signal collected, but also decreases the nonspecific adsorption effect after the hybridization	[25]
Fe_3O_4/ZnO/Au nanorices	Anti-IgG	Human IgG	Raman	[DL]: 2 fM	[92]
ZnONPs	Anti-IgG	Rabbit IgG	SPR	[L]: 0.15–20 μg mL^{-1}	[36]
ZnONPs	Anti-IgM	Human IgM	Surface Plasmon Resonance	[DR]: 0.30–20.00 μg mL^{-1}	[91]
ZnONP	Lactate	Lactate oxidase	Electrochemiluminescence	[L]: 0.01–10 μmol L^{-1} and 10–200 μmol L^{-1}; [DL]: 4 nmol L^{-1}	[200]
Nanostructured ZnO film	GOx	Glucose	SPR	[L]: 50–250 ng mL^{-1}	[151]
ZnONR	Citrullinated peptide	Rheumatoid arthritis	Fluorescence	Detection upto 5000 times diluted patient serum	[94]
ZnONR	Anti-CEA or anti-α-fetoprotein	CEA or α-fetoprotein	Fluorescence	[DL]: 1 pg mL^{-1}	[93]
ZnONR	Biotin	Streptavidin	FET	[L]: 25–250 nM; [DL]: 25 nM, single molecular detection level	[159]
ZnONW	Biotin	Streptavidin	FET	[L]: 2.5–250 nM; [DL]: 2.5 nM	[201]
ZnONW	GOx	Glucose	MOSFET	[DR]: 1–100 μM; [RT]: 100 ms	[77]
ZnO nanothin film	Riboflavin aptamer	Riboflavin	FET	[DL]: 1 pM	[202]
ZnONR	GOx	Glucose	Extended Gate FET	[L]: 0–10 mM; [RT]: 10 s; [S]: 20.33 μA mM^{-1} cm^{-2}	[203]
ZnO nano thin film	Anti-EGFR	EGFR	TFT	[L]: 10 fM–10 nM; [DL]: 10 fM	[132]

mechanical energy and vice versa. The enhanced sensitivity of SAW over QCM based biosensors is typically attributed to the fact that the acoustic energy of SAW based biosensors is confined in the surface layer of approximately one wavelength. The base mass of the active layer is smaller by one order of magnitude than that of QCM, thus increasing the sensitivity of SAW devices dramatically compared to QCM. SAWs devices normally use one or more interdigitated electrodes (IDTs) to convert acoustic waves to electrical signals and vice versa by exploiting the piezoelectric effect of certain materials. SAW devices can be used in higher operating frequencies than other devices. In SAW devices, waves exist on the surface and propagate as Rayleigh waves. These waves in the SAW device are generated by applying a voltage on IDTs deposited on a piezoelectric substrate like ZnO. The wave confined to the surface travels through the SAW device and the acoustic energy is collected by another set of IDTs. The frequency of the propagating wave is determined by the IDT spacing. Any mass loading on the piezoelectric surface in the region of propagation causes a change in the frequency and provides a platform for using these devices as sensors [8,206]. The first trials of SAW devices as chemical sensors in liquid media were not highly successful due to the great attenuation of Rayleigh waves in liquid [207]. However, this problem was overcome using a surface transverse wave (STW), or a shear horizontal SAW device [208,209]. Recently, ZnO possessing good piezoelectric properties has been used as part of SAW based biosensors. Zhang et al. developed a structure consisting of ZnO nanotips on Y-cut $LiNbO_3$ onto which oligonucleotide probes were immobilized and hybridized. The probe-binding capacity of the device was found to be 2.2×10^{-3} g cm^{-2} and 1.5 g cm^{-2} after hybridization, indicating a promising potential for designing portable sensors for chemical and biomedical applications [6]. A novel high sensitivity $ZnO/SiO_2/Si$ Love mode SAW biosensor for the detection of IL-6 has been reported and binding of the antibody through direct surface adsorption versus covalent binding is presented. The biosensor was denoted as having extended linearity, which improved with higher frequency [170].

In addition to QCM and SAW devices, film bulk acoustic resonator or flexural plate wave also uses the piezoelectric properties of ZnO for biosensing. Devices based on FBAR and FPW are in their infancy and making their way toward biosensing applications. These devices have piezoelectric film sandwiched between two electrodes and a mechanical motion is produced with rf power applied across the film thickness. A frequency resonance is achieved when the film thickness is double the wavelength of the input rf signal. Because the resonant frequency depends on the material property, any change in the mass can be detected as a frequency shift. The affinity biosensors exploit this resonance shift due to mass loading for sensing applications. Recently, Wingqvist described the developments in shear mode FBAR technology developments and the investigations of the shear mode FBAR biosensor technology with regard to sensitivity, resolution and detection distance [210]. Yan et al. described the fabrication of a ZnO based FBAR by magnetron sputtering with a resonant frequency of 3–4 GHz. The sensitivity of the device has been reported as 8–10 kHz cm^2 ng^{-1} and has been claimed to be a protein detector with a mass sensitivity one thousand times better than that of QCM [211,212]. Gabl et al. reported the feasibility of a label-free DNA biosensor based on thin film FBAR, where they integrated ZnO bulk acoustic wave resonators with resonance frequencies of approximately 2 GHz [213]. Dickherber et al. have reported a performance optimization of ZnO FBARs for biosensors operating in thickness shear mode through the characterization of a variety of electrode geometries [214]. Huang et al. developed an allergy biosensor based on a $Si/SiO_2/Si_3N_4/Cr/Au/ZnO$ floating thin film. The FPW transducer with immobilized IgE antibody exhibited high sensitivity toward mass loading via IgE antigen binding [157].

5. Vision on ZnO based biosensors

The ability to grow well controlled ZnO nanostructures for various bio-applications involving enzymes, proteins, DNA, etc. and its capability of integrating to the CMOS and MEMS devices makes ZnO a promising material for point of care devices and for futuristic telemedicine's. Capitalizing on its high isoelectric point, charge transfer properties, biocompatibility, ease of synthesis and surface to volume ratio, ZnO nanostructures possess advantage over nanostructures of other materials. Further, the easy modification via surface functionalization makes ZnO nanostructures useful for number of technological applications.

As clear from the above discussion and collective work of various groups, ZnO nanostructures for biosensor application can be prepared using different procedures and via slight modification of growth conditions. Among various growth procedures wet chemical methods provide growth of a variety of ZnO nanostructures easily at low temperature conditions. However, uniformity of structure and reproducibility in different batches is an issue as even very slight change in conditions such as temperature, pH, analyte concentration, time, etc. can leads to different morphology. On the other hand, physical methods of growth have advantage of reproducibility and uniformity. However, they need harsh growth condition and not suitable for growth on large size wafer scale. The electrochemical methods are comparably better choice for direct growth of ZnO nanostructure on electrode surface in doped or undoped form.

ZnO composite with cobalt and gold has shown promise for high adsorption, high electro-catalytic activity, high biocompatibility and direct electrochemistry. Thinner and multidirectional ZnO nanostructures have provided better solution for higher loading of biomolecules and direct transfer of electrons. Moreover use of ZnO in biosensor is advantageous because it can be prepared in large number of nanostructures in easy manner, it possess high isoelectric point resulting in easy and stronger binding of various biomolecule on its surface, good biocompatibility and faster charge transfer property, which makes it suitable for electrochemical biosensors. Further fluorescence and piezoelectric properties makes it suitable for use in fabrication of sensitive optical and piezoelectric biosensor. Unlike ZnO, other promising materials, e.g., CNTs and gold nanostructures normally only have a limited range of structures available for biosensor construction. Further insufficient knowledge about interaction between ZnO and bound biomolecule put limitation for commercial development of ZnO based biosensor. However such limitation can be overcome by improving ZnO-biomolecule interface understanding via investigating their optical and electrochemical behavior under the influence of various external environmental and physical conditions.

For technological application in biosensor, it is advantageous to grow ZnO nanostructure directly on electrode surface uniformly and repeatable manner. Such ZnO based platform can be employed as immobilization matrix to construct electrochemical biosensor for detection of biologically important analytes such as DNA, metabolites, cancer markers, etc. and can have implication in clinical diagnosis and proteomics. Use of such platform will lead to fabrication of viable commercial electrochemical biosensor and point of care measurement. It is anticipated that ZnO based biosensor will soon lead to decisive improvement in quality of human life.

6. Challenges

Following above discussion, it is clear that several fabrication procedure and experience already exists in various laboratories, the current challenge is to produce large quantities of 1D ZnO nanostructures with well-controlled dimensions and

morphologies. Further dedicated efforts are needed for fabrication of application specific different type of ZnO nanostructure reproducibly. Additional facilities and development efforts are necessary for integrating the fabricated ZnO nanostructures with commercial detection systems for their real application in biosensor and healthcare field. Moreover, the interaction of 1D ZnO nanostructures with a variety of biomolecules needs more extensive study.

7. Summary

The widespread interest in nanostructured materials over the past decade has resulted from the development of novel synthesis methods and better characterization techniques that allowed the creation of new functionalities. These nanostructures, due to their remarkable variations in fundamental electrical, optical and physico-chemical properties, showed great promise for faster responses and higher sensitivity compared to planar configurations in biosensor applications.

Nanostructured ZnO had proven its potential as a biomaterial for biosensing applications. This extensive review on ZnO nanostructures as a biosensor matrix material highlights the various procedures that can be employed for the formation and the applicability of ZnO structures in biomolecule immobilization. The ease of fabrication using low-cost processes, which can yield a myriad of nanostructures, makes ZnO based matrices a promising platform for low-cost biosensors. Moreover, the biocompatible nature of ZnO and compatibility with MEMS technology will play a major role in the use of this material in designing miniaturized, wireless and implantable biosensors. Furthermore, doping of ZnO with noble metals offers an effective approach to the enhance physico-chemical properties of nanostructures, which is crucial for their practical application. It is not possible to address all of the recent works in this review. However, we have attempted to cover most ZnO nanostructure and thin film based biosensors, considering the morphological aspects along with various transduction techniques including piezoelectric, electrochemical, optical and field effect transistor based detection.

Acknowledgments

SPS acknowledges the support from Director, NPL, New Delhi, India. The IFN-NSF-EPSCoRE start-up grant OIA-0701525 is also gratefully acknowledged. S.K.A. acknowledges a post-doctoral fellowship from USF, Tampa.

References

[1] M. Frasconi, G. Favero, M. Di Fusco, F. Mazzei, Biosens. Bioelectron. 24 (2009) 1424.
[2] S. Krishnamoorthy, A.A. Iliadis, Solid-State Electron. 52 (2008) 1710.
[3] H.Y. Park, H.Y. Go, S. Kalme, R.S. Mane, S.H. Han, M.Y. Yoon, Anal. Chem. 81 (2009) 4280.
[4] C. Klingshirn, Phys. Stat. Solid. B 244 (2007) 3027.
[5] U. Ozgur, Y.I. Alivov, C. Liu, A. Teke, M.A. Reshchikov, S. Dogan, V. Avrutin, S.J. Cho, H. Morkoc, J. Appl. Phys. 98 (2005) 041301.
[6] Z. Zhang, N.W. Emanetoglu, G. Saraf, Y.M. Chen, P. Wu, J. Zhong, Y.C. Lu, J.Q. Chen, O. Mirochnitchenko, M. Inouye, IEEE Trans. Ultrason. Ferroelectr. Frequency Control 53 (2006) 786.
[7] A. Ashrafi, C. Jagadish, J. Appl. Phys. 102 (2007) 071101.
[8] Y.Q. Fu, J.K. Luo, X.Y. Du, A.J. Flewitt, Y. Li, G.H. Markx, A.J. Walton, W.I. Milne, Sens. Actuat. B: Chem. 143 (2010) 606.
[9] Z.L. Wang, J. Phys.-Condens. Mat. 16 (2004) R829.
[10] Y.-B. Hahn, Korean J. Chem. Eng. 28 (2011) 1797.
[11] A. Wei, L. Pan, W. Huang, Mater. Sci. Eng.: B 176 (2011) 1409.
[12] M. Ahmad, J. Zhu, J. Mater. Chem. 21 (2011) 599.
[13] X.-Y. Ma, W.-D. Zhang, Polym. Degrad. Stab. 94 (2009) 1103.
[14] X. Wang, F. Yang, W. Yang, X. Yang, Chem. Commun. (2007) 4419.
[15] Q. Li, S. Mahendra, D.Y. Lyon, L. Brunet, M.V. Liga, D. Li, P.J.J. Alvarez, Water Res. 42 (2008) 4591.
[16] C. Hanley, J. Layne, A. Punnoose, K.M. Reddy, I. Coombs, A. Coombs, K. Feris, D. Wingett, Nanotechnology 19 (2008) 295103.
[17] P. Joshi, S. Chakraborti, P. Chakrabarti, D. Haranath, V. Shanker, Z.A. Ansari, S.P. Singh, V. Gupta, J. Nanosci. Nanotechnol. 9 (2009) 6427.
[18] V. Gupta, Thin Solid Films 519 (2010) 1141.
[19] C.G. Allen, D.J. Baker, J.M. Albin, H.E. Oertli, D.T. Gillaspie, D.C. Olson, T.E. Furtak, R.T. Collins, Langmuir 24 (2008) 13393.
[20] M. Ahmad, C. Pan, Z. Luo, J. Zhu, J. Phys. Chem. C 114 (2010) 9308.
[21] A. Fulati, S.M.U. Ali, M.H. Asif, N.u.H. Alvi, M. Willander, C. Brännmark, P. Strålfors, S.I. Börjesson, F. Elinder, B. Danielsson, Sens. Actuat. B: Chem. 150 (2010) 673.
[22] M. Ahmad, C. Pan, L. Gan, Z. Nawaz, J. Zhu, J. Phys. Chem. C 114 (2009) 243.
[23] G.-Q. Mo, J.-S. Ye, W.-D. Zhang, Electrochim. Acta 55 (2009) 511.
[24] M. Ahmad, C. Pan, J. Iqbal, L. Gan, J. Zhu, Chem. Phys. Lett. 480 (2009) 105.
[25] J. Zhao, L. Wu, J. Zhi, J. Mater. Chem. 18 (2008) 2459.
[26] B. Gu, C. Xu, C. Yang, S. Liu, M. Wang, Biosens. Bioelectron. 26 (2011) 2720.
[27] J. Weber, S. Jeedigunta, A. Kumar, J. Nanomater. 2008 (2008) Article ID 638523.
[28] M. Willander, P. Klason, L.L. Yang, S.M. Al-Hilli, Q.X. Zhao, O. Nur, Phys. Stat.Solid. (c) 5 (2008) 3076.
[29] X. Liu, Q. Hu, Q. Wu, W. Zhang, Z. Fang, Q. Xie, Colloids Surf. B: Biointerfac. 74 (2009) 154.
[30] Y. Lei, X. Yan, J. Zhao, X. Liu, Y. Song, N. Luo, Y. Zhang, Colloids Surf. B: Biointerfac. 82 (2011) 168.
[31] X.W. Sun, J.X. Wang, A. Wei, J. Mater. Sci. Technol. 24 (2008) 649.
[32] J.X. Wang, X.W. Sun, A. Wei, Y. Lei, X.P. Cai, C.M. Li, Z.L. Dong, Appl. Phys. Lett. 88 (2006) 233106.
[33] Z. Yang, X. Zong, Z. Ye, B. Zhao, Q. Wang, P. Wang, Biomaterials 31 (2010) 7534.
[34] C. Xia, N. Wang, L. Lidong, G. Lin, Sens. Actuat. B: Chem. 129 (2008) 268.
[35] Z. Yang, Z. Ye, B. Zhao, X. Zong, P. Wang, J. Sol-Gel Sci. Technol. 54 (2010) 282.
[36] L. Wang, Y. Sun, J. Wang, J. Wang, A. Yu, H. Zhang, D. Song, J. Colloid Interface Sci. 351 (2010) 392.
[37] Y. Lei, X. Yan, N. Luo, Y. Song, Y. Zhang, Colloids Surf. A: Physicochem. Eng. Aspects 361 (2010) 169.
[38] Z.H. Dai, K. Liu, Y.W. Tang, X.D. Yang, J.C. Bao, J. Shen, J. Mater. Chem. 18 (2008) 1919.
[39] Y.-T. Wang, L. Yu, Z.-Q. Zhu, J. Zhang, J.-Z. Zhu, C.-h. Fan, Sensors Actuat. B: Chem. 136 (2009) 332.
[40] X. Zhu, I. Yuri, X. Gan, I. Suzuki, G. Li, Biosens. Bioelectron. 22 (2007) 1600.
[41] S.A. Ansari, Q. Husain, S. Qayyum, A. Azam, Food Chem. Toxicol. 49 (2011) 2107.
[42] X. Feng, Y. Liu, Q. Kong, J. Ye, X. Chen, J. Hu, Z. Chen, J. Solid State Electrochem. 14 (2010) 923.
[43] T. Kong, Y. Chen, Y. Ye, K. Zhang, Z. Wang, X. Wang, Sens. Actuat. B: Chem. 138 (2009) 344.
[44] K. Yang, G.-W. She, H. Wang, X.-M. Ou, X.-H. Zhang, C.-S. Lee, S.-T. Lee, J. Phys. Chem. C 113 (2009) 20169.
[45] S.G. Ansari, R. Wahab, Z.A. Ansari, Y.-S. Kim, G. Khang, A. Al-Hajry, H.-S. Shin, Sens. Actuat. B: Chem. 137 (2009) 566.
[46] D. Pradhan, Z. Su, S. Sindhwani, J.F. Honek, K.T. Leung, J. Phys. Chem. C 115 (2011) 18149.
[47] C. Xia, W. Ning, W. Long, G. Lin, Sens. Actuat. B-Chem. 147 (2010) 629.
[48] A. Umar, M.M. Rahman, A. Al-Hajry, Y.B. Hahn, Talanta 78 (2009) 284.
[49] C. Xiang, Y. Zou, L.-X. Sun, F. Xu, Sens. Actuat. B: Chem. 136 (2009) 158.
[50] X. Lu, H. Zhang, Y. Ni, Q. Zhang, J. Chen, Biosens. Bioelectron. 24 (2008) 93.
[51] Q. Rui, K. Komori, Y. Tian, H. Liu, Y. Luo, Y. Sakai, Anal. Chim. Acta 670 (2010) 57.
[52] Z. Deng, Q. Rui, X. Yin, H. Liu, Y. Tian, Anal. Chem. 80 (2008) 5839.
[53] P.R. Solanki, A. Kaushik, A.A. Ansari, B.D. Malhotra, Appl. Phys. Lett. 94 (2009) 3.
[54] A. Ali, A.A. Ansari, A. Kaushik, P.R. Solanki, A. Barik, M.K. Pandey, B.D. Malhotra, Mater. Lett. 63 (2009) 2473.
[55] S.P. Singh, S.K. Arya, P. Pandey, B.D. Malhotra, S. Saha, K. Sreenivas, V. Gupta, Appl. Phys. Lett. 91 (2007) 3.
[56] J.P. Liu, X.T. Huang, Y.Y. Li, X.X. Ji, Z.K. Li, X. He, F.L. Sun, J. Phys. Chem. C 111 (2007) 4990.
[57] L.E. Greene, B.D. Yuhas, M. Law, D. Zitoun, P.D. Yang, Inorg. Chem. 45 (2006) 7535.
[58] Z.R. Tian, J.A. Voigt, J. Liu, B. McKenzie, M.J. McDermott, J. Am. Chem. Soc. 124 (2002) 12954.
[59] H. Hu, C. Deng, X. Huang, Mater. Chem. Phys. 121 (2010) 364.
[60] H. Zhang, D. Yang, S. Li, X. Ma, Y. Ji, J. Xu, D. Que, Mater. Lett. 59 (2005) 1696.
[61] S.M.U. Ali, T. Aijazi, K. Axelsson, O. Nur, M. Willander, Sensors-Basel 11 (2011) 8485.
[62] R. Razali, A.K. Zak, W.H.A. Majid, M. Darroudi, Ceram. Int. 37 (2011) 3657.
[63] G. Du, L. Zhang, Y. Feng, Y. Xu, Y. Sun, B. Ding, Q. Wang, Mater. Lett. 73 (2012) 86.
[64] B. Zhao, H. Chen, Mater. Lett. 61 (2007) 4890.
[65] L. Yang, D. Qiu, F. Yu, S. Chen, Y. Yin, Mater. Sci. Semicond. Process. 14 (2011) 193.
[66] G. Amin, M.H. Asif, A. Zainelabdin, S. Zaman, O. Nur, M. Willander, J. Nanomater. 2011 (2011) Article ID 269692.
[67] M.Q. Israr, J.R. Sadaf, M.H. Asif, O. Nur, M. Willander, B. Danielsson, Thin Solid Films 519 (2010) 1106.
[68] M. Mehrabian, R. Azimirad, K. Mirabbaszadeh, H. Afarideh, M. Davoudian, Phys. E: Low-dimension. Syst. Nanostruct. 43 (2011) 1141.
[69] B.X. Gu, C.X. Xu, G.P. Zhu, S.Q. Liu, L.Y. Chen, X.S. Li, J. Phys. Chem. B 113 (2008) 377.

[70] A. Wei, X.W. Sun, J.X. Wang, Y. Lei, X.P. Cai, C.M. Li, Z.L. Dong, W. Huang, Appl. Phys. Lett. 89 (2006) 123902.
[71] Y.-L. Liu, Y.-H. Yang, H.-F. Yang, Z.-M. Liu, G.-L. Shen, R.-Q. Yu, J. Inorg. Biochem. 99 (2005) 2046.
[72] Y.-F. Li, Z.-M. Liu, Y.-L. Liu, Y.-H. Yang, G.-L. Shen, R.-Q. Yu, Anal. Biochem. 349 (2006) 33.
[73] Y. Zhang, Y. Zhang, H. Wang, B. Yan, G. Shen, R. Yu, J. Electroanal. Chem. 627 (2009) 9.
[74] L. Yu, F. Qu, X. Wu, Appl. Surf. Sci. 257 (2011) 7432.
[75] Z.H. Dai, G.J. Shao, J.M. Hong, J.C. Bao, J. Shen, Biosens. Bioelectron. 24 (2009) 1286.
[76] Z. Yang, Z. Ye, B. Zhao, X. Zong, P. Wang, Phys. E: Low-dimens. Syst. Nanostruct. 42 (2010) 1830.
[77] S.M.U. Ali, O. Nur, M. Willander, B. Danielsson, IEEE Trans. Nanotechnol. 8 (2009) 678.
[78] S.M.U. Ali, O. Nur, M. Willander, B. Danielsson, Sens. Actuat. B-Chem. 145 (2010) 869.
[79] D. Lee, M. Yoo, H. Seo, Y. Tak, W.-G. Kim, K. Yong, S.-W. Rhee, S. Jeon, Sens. Actuat. B: Chem. 135 (2009) 444.
[80] J.P. Cheng, X.B. Zhang, Z.Q. Luo, Surf. Coat. Tech. 202 (2008) 4681.
[81] X. Yan, Z. Li, C. Zou, S. Li, J. Yang, R. Chen, J. Han, W. Gao, J. Phys. Chem. C 114 (2010) 1436.
[82] B. Fang, C. Zhang, G. Wang, M. Wang, Y. Ji, Sens. Actuat. B: Chem. 155 (2011) 304.
[83] X. Hou, F. Zhou, Y. Sun, W. Liu, Mater. Lett. 61 (2007) 1789.
[84] M. Chen, Z. Wang, D. Han, F. Gu, G. Guo, Sens. Actuat. B: Chem. 157 (2011) 565.
[85] J. Liu, C. Guo, C.M. Li, Y. Li, Q. Chi, X. Huang, L. Liao, T. Yu, Electrochem. Commun. 11 (2009) 202.
[86] A. Umar, M.M. Rahman, M. Vaseem, Y.-B. Hahn, Electrochem. Commun. 11 (2009) 118.
[87] W. Zhang, T. Yang, D. Huang, K. Jiao, G. Li, J. Membr. Sci. 325 (2008) 245.
[88] G. Duan, Y. Li, Y. Wen, X. Ma, Y. Wang, J. Ji, P. Wu, Z. Zhang, H. Yang, Electroanalysis 20 (2008) 2454.
[89] X. Ren, D. Chen, X. Meng, F. Tang, X. Hou, D. Han, L. Zhang, J. Colloid Interface Sci. 334 (2009) 183.
[90] C. Yang, B. Gu, C. Xu, X. Xu, J. Electroanal. Chem. 660 (2011) 97.
[91] L. Wang, J. Wang, S. Zhang, Y. Sun, X. Zhu, Y. Cao, X. Wang, H. Zhang, D. Song, Anal. Chim. Acta 653 (2009) 109.
[92] X. Hong, X. Chu, P. Zou, Y. Liu, G. Yang, Biosens. Bioelectron. 26 (2010) 918.
[93] W. Hu, Y. Liu, H. Yang, X. Zhou, C.M. Li, Biosens. Bioelectron. 26 (2011) 3683.
[94] K.-Y. Ahn, K. Kwon, J. Huh, G.T. Kim, E.B. Lee, D. Park, J. Lee, Biosens. Bioelectron. 28 (2011) 378.
[95] A. Pezzulo, M. Asif, M. Willander, J. Zabner, J. Anal. Bioanal. Techn. S7:002 (2011) http://dx.doi.org/10.4172/2155.
[96] S.M.U. Ali, M. Kashif, Z.H. Ibupoto, M. Fakhar-e-Alam, U. Hashim, M. Willander, Micro & Nano Lett. 6 (2011) 609.
[97] J. Narang, C.S. Pundir, Int. J. Biol. Macromol. 49 (2011) 707.
[98] S. Yadav, R. Devi, A. Kumar, C.S. Pundir, Biosens. Bioelectron. 28 (2011) 64.
[99] R. Devi, M. Thakur, C.S. Pundir, Biosens. Bioelectron. 26 (2011) 3420.
[100] M.Q. Israr, J.R. Sadaf, O. Nur, M. Willander, S. Salman, B. Danielsson, Appl. Phys. Lett. 98 (2011) 253705.
[101] W. Tu, J. Lei, P. Wang, H. Ju, Chem.–A Eur. J. 17 (2011) 9440.
[102] B.W. Chieng, Y.Y. Loo, Mater. Lett. 73 (2012) 78.
[103] M. Caglar, S. Ilican, Y. Caglar, F. Yakuphanoglu, J. Alloys Compd. 509 (2011) 3177.
[104] F. Yakuphanoglu, Y. Caglar, M. Caglar, S. Ilican, Mater. Sci. Semicond. Process. 13 (2010) 137.
[105] N. Ye, C.C. Chen, Opt. Mater. 34 (2012) 753.
[106] S.-K. Min, R.S. Mane, O.-S. Joo, T. Ganesh, B.W. Cho, S.-H. Han, Curr. Appl. Phys. 9 (2009) 492.
[107] Z. Zhu, D. Yang, H. Liu, Adv. Powder Technol. 22 (2011) 493.
[108] B.C. Yadav, R. Srivastava, C.D. Dwivedi, P. Pramanik, Sens. Actuat. A: Phys. 153 (2009) 137.
[109] Y. Zeng, Z. Lou, L. Wang, B. Zou, T. Zhang, W. Zheng, G. Zou, Sens. Actuat. B: Chem. 156 (2011) 395.
[110] A. Yu, J. Qian, H. Pan, Y. Cui, M. Xu, L. Tu, Q. Chai, X. Zhou, Sens. Actuat. B: Chem. 158 (2011) 9.
[111] A. Phuruangrat, T. Thongtem, S. Thongtem, Mater. Lett. 63 (2009) 1224.
[112] C. Chen, P. Liu, C. Lu, Chem. Eng. J. 144 (2008) 509.
[113] S.-J. Bao, C.M. Li, J.-F. Zang, X.-Q. Cui, Y. Qiao, J. Guo, Adv. Funct. Mater. 18 (2008) 591.
[114] M. Salavati-Niasari, F. Davar, A. Khansari, J. Alloys Compd. 509 (2011) 61.
[115] C. Yang, C. Xu, X. Wang, Langmuir 28 (2012) 4580.
[116] J.-M. Jang, C.-R. Kim, H. Ryu, M. Razeghi, W.-G. Jung, J. Alloys Compd. 463 (2008) 503.
[117] W. Peng, S. Qu, G. Cong, Z. Wang, Cryst. Growth Des. 6 (2006) 1518.
[118] X.D. Guo, H.Y. Pi, Q.Z. Zhao, R.X. Li, Mater. Lett. 66 (2012) 377.
[119] X. Wei, H. Li, C.e. Yuan, Q. Li, S. Chen, Micropor. Mesopor. Mater. 118 (2009) 307.
[120] B. Krishnan, L. Irimpan, V.P.N. Nampoor, V. Kumar, Phys. E: Low-dimension. Syst. Nanostruct. 40 (2008) 2787.
[121] X. Jiang, Y. Liu, Y. Gao, X. Zhang, L. Shi, Particuology 8 (2010) 383.
[122] C. Liangyuan, L. Zhiyong, B. Shouli, Z. Kewei, L. Dianqing, C. Aifan, C.C. Liu, Sens. Actuat. B: Chem. 143 (2010) 620.
[123] S. Tan, X. Tan, J. Jiang, J. Xu, J. Zhang, D. Zhao, L. Liu, Z. Huang, J. Electroanal. Chem. 668 (2012) 113.
[124] J. Wang, S. Li, Y. Zhang, Electrochim. Acta 55 (2010) 4436.
[125] J.S. Jeong, J.Y. Lee, Nanotechnology 21 (2010) 475603.
[126] L. Chen, B. Gu, G. Zhu, Y. Wu, S. Liu, C. Xu, J. Electroanal. Chem. 617 (2008) 7.
[127] Y.T. Wang, L. Yu, J. Wang, L. Lou, W.J. Du, Z.Q. Zhu, H. Peng, J.Z. Zhu, J. Electroanal. Chem. 661 (2011) 8.
[128] O. Taratula, E. Galoppini, R. Mendelsohn, P.I. Reyes, Z. Zhang, Z. Duan, J. Zhong, Y. Lu, Langmuir 25 (2009) 2107.
[129] P.I. Reyes, Z. Zheng, C. Hanhong, D. Ziqing, Z. Jian, G. Saraf, L. Yicheng, O. Taratula, E. Galoppini, N.N. Boustany, Sens. J. IEEE 9 (2009) 1302.
[130] S.-S. Lin, I.C. Chen, J. Yang, T.J. Hsueh, C.-L. Hsu, H.-E. Lee, T.-Y. Shieh, J. Electrochem. Soc. 158 (2011) K107.
[131] S. Saha, V. Gupta, J. Appl. Phys. 110 (2011) 064904.
[132] P.I. Reyes, C.-J. Ku, Z. Duan, Y. Lu, A. Solanki, K.-B. Lee, Appl. Phys. Lett. 98 (2011) 173702.
[133] S. Venkatachalam, Y. Kanno, Curr. Appl. Phys. 9 (2009) 1232.
[134] O. Takai, M. Futsuhara, G. Shimizu, C.P. Lungu, J. Nozue, Thin Solid Films 318 (1998) 117.
[135] Q. Wan, K. Yu, T.H. Wang, C.L. Lin, Appl. Phys. Lett. 83 (2003) 2253.
[136] S.H. Huang, Z. Chen, X.C. Shen, Z.Q. Zhu, K. Yu, Solid State Commun. 145 (2008) 418.
[137] WangWang, C.J. Summers, Z.L. Wang, Nano Lett. 4 (2004) 423.
[138] T.-J. Hsueh, C.-L. Hsu, Sens. Actuat. B: Chem. 131 (2008) 572.
[139] H. Cheng, J. Cheng, Y. Zhang, Q.-M. Wang, J. Cryst. Growth 299 (2007) 34.
[140] Z.F. Wu, X.M. Wu, L.J. Zhuge, B. Hong, X.M. Yang, T. Yu, J.J. He, Q. Chen, Appl. Surf. Sci. 256 (2010) 2259.
[141] H. Kim, J. Moon, H. Lee, Electron. Mater. Lett. 7 (2011) 59.
[142] A. Stafiniak, B. Boratyński, A. Baranowska-Korczyc, A. Szyszka, M. Ramiączek-Krasowska, J. Prażmowska, K. Fronc, D. Elbaum, R. Paszkiewicz, M. Tłaczała, Sens. Actuat. B: Chem. 160 (2011) 1413.
[143] Y. Leprince-Wang, S. Bouchaib, T. Brouri, M. Capo-Chichi, K. Laurent, J. Leopoldes, S. Tusseau-Nenez, L. Lei, Y. Chen, Mater. Sci. Eng.: B 170 (2010) 107.
[144] Y. Leprince-Wang, A. Yacoubi-Ouslim, G.Y. Wang, Microelectron. J. 36 (2005) 625.
[145] H.P. Bai, X.X. Lu, G.M. Yang, Y.H. Yang, Chin. Chem. Lett. 19 (2008) 314.
[146] G.W. She, X.H. Zhang, W.S. Shi, X. Fan, J.C. Chang, Electrochem. Commun. 9 (2007) 2784.
[147] C. Zhang, G. Wang, M. Liu, Y. Feng, Z. Zhang, B. Fang, Electrochimica. Acta 55 (2010) 2835.
[148] F. Hu, S. Chen, C. Wang, R. Yuan, Y. Chai, Y. Xiang, C. Wang, J. Mol. Catal. B: Enzym. 72 (2011) 298.
[149] G. Zhao, J.-J. Xu, H.-Y. Chen, Anal. Biochem. 350 (2006) 145.
[150] M. Das, G. Sumana, R. Nagarajan, B.D. Malhotra, Thin Solid Films 519 (2010) 1196.
[151] N.K. Singh, B. Jain, S. Annapoorni, Sens. Actuat. B: Chem. 156 (2011) 383.
[152] B. Xue, Y. Liang, L. Donglai, N. Eryong, S. Congli, F. Huanhuan, X. jingjing, J. Yong, J. Zhifeng, S. Xiaosong, Appl. Surf. Sci. 257 (2011) 10317.
[153] E. Topoglidis, A.E.G. Cass, B. O'Regan, J.R. Durrant, J. Electroanal. Chem. 517 (2001) 20.
[154] L. Nie, L.Z. Gao, X.Y. Yan, T.H. Wang, Nanotechnology 18 (2007).
[155] J. Zhao, J. Zhi, Y. Zhou, W. Yan, Anal. Sci. 25 (2009) 1083.
[156] Y. Wei, Y. Li, X. Liu, Y. Xian, G. Shi, L. Jin, Biosens. Bioelectron. 26 (2010) 275.
[157] I.Y. Huang, M.C. Lee, Sens. Actuat. B: Chem. 132 (2008) 340.
[158] F.F. Zhang, X.L. Wang, S.Y. Ai, Z.D. Sun, Q. Wan, Z.Q. Zhu, Y.Z. Xian, L.T. Jin, K. Yamamoto, Anal. Chim. Acta 519 (2004) 155.
[159] J.S. Kim, W. Il Park, C.H. Lee, G.C. Yi, J. Korean Phys. Soc. 49 (2006) 1635.
[160] L. Armelao, M. Pascolini, E. Biasiolo, E. Tondello, G. Bottaro, M.D. Carbonare, A. D'Arrigo, A. Leon, Inorg. Chim. Acta 361 (2008) 3603.
[161] S. Krishnamoorthy, T. Bei, E. Zoumakis, G.P. Chrousos, A.A. Iliadis, Biosens. Bioelectron. 22 (2006) 707.
[162] Z.W. Zhao, X.J. Chen, B.K. Tay, J.S. Chen, Z.J. Han, K.A. Khor, Biosens. Bioelectron. 23 (2007) 135.
[163] C.D. Corso, A. Dickherber, W.D. Hunt, Biosens. Bioelectron. 24 (2008) 805.
[164] W. Ma, W. Song, D.B. Tian, Chin. Chem. Lett. 20 (2009) 358.
[165] W. Ma, D.B. Tian, Bioelectrochemistry 78 (2010) 106.
[166] S. Saha, S.K. Arya, S.P. Singh, K. Sreenivas, B.D. Malhotra, V. Gupta, Thin Solid Films 519 (2010) 1184.
[167] Z. Liu, Y. Liu, H. Yang, Y. Yang, G. Shen, R. Yu, Electroanalysis 17 (2005) 1065.
[168] M. Yang, Y. Yang, Y. Yang, G. Shen, R. Yu, Anal. Chim. Acta 530 (2005) 205.
[169] C.-C. Chang, N.-F. Chiu, D.S. Lin, Y. Chu-Su, Y.-H. Liang, C.-W. Lin, Anal. Chem. 82 (2010) 1207.
[170] S. Krishnamoorthy, A.A. Iliadis, T. Bei, G.P. Chrousos, Biosens. Bioelectron. 24 (2008) 313.
[171] Z. Zhao, W. Lei, X. Zhang, B. Wang, H. Jiang, Sensors-Basel 10 (2010) 1216.
[172] A. Heller, Acc. Chem. Res. 23 (1990) 128.
[173] S. Borgmann, G. Hartwich, A. Schulte, W. Schuhmann, in: F.S. Emil Paleček, J. Wang (Eds.), Perspectives in Bioanalysis, Elsevier, 2005, p. 599.
[174] A.L. Ghindilis, P. Atanasov, E. Wilkins, Electroanalysis 9 (1997) 661.
[175] L. Gorton, A. Lindgren, T. Larsson, F.D. Munteanu, T. Ruzgas, I. Gazaryan, Anal. Chim. Acta 400 (1999) 91.
[176] A. Christenson, N. Dimcheva, E.E. Ferapontova, L. Gorton, T. Ruzgas, L. Stoica, S. Shleev, A.I. Yaropolov, D. Haltrich, R.N.F. Thorneley, S.D. Aust, Electroanalysis 16 (2004) 1074.

[177] Z. Wang, M. Li, P. Su, Y. Zhang, Y. Shen, D. Han, A. Ivaska, L. Niu, Electrochem. Commun. 10 (2008) 306.
[178] X. Zhao, Z. Mai, X. Kang, X. Zou, Biosens. Bioelectron. 23 (2008) 1032.
[179] J.-T. Zhu, C.-G. Shi, J.-J. Xu, H.-Y. Chen, Bioelectrochemistry 71 (2007) 243.
[180] H. Zhou, T.-H. Lu, H.-X. Shi, Z.-H. Dai, X.-H. Huang, J. Electroanal. Chem. 612 (2008) 173.
[181] M. Yang, F. Qu, Y. Li, Y. He, G. Shen, R. Yu, Biosens. Bioelectron. 23 (2007) 414.
[182] Y. Xiao, C.M. Li, Electroanalysis 20 (2008) 648.
[183] Z. Dai, G. Shao, J. Hong, J. Bao, J. Shen, Biosens. Bioelectron. 24 (2009) 1286.
[184] H. Fatemi, A.A. Khodadadi, A. Anaraki Firooz, Y. Mortazavi, Curr. Appl. Phys. 12 (2012) 1033.
[185] Z. Deng, Y. Tian, X. Yin, Q. Rui, H. Liu, Y. Luo, Electrochem. Commun. 10 (2008) 818.
[186] R. Khan, A. Kaushik, P.R. Solanki, A.A. Ansari, M.K. Pandey, B.D. Malhotra, Anal. Chim. Acta 616 (2008) 207.
[187] Y.H. Yang, M.H. Yang, J.H. Jlang, G.L. Shen, R.Q. Yu, Chin. Chem. Lett. 16 (2005) 951.
[188] C.L. Zhang, M.C. Liu, P. Li, Y.Z. Xian, Y.X. Cheng, F.F. Zhang, X.L. Wang, L.T. Jin, Chin. J. Chem. 23 (2005) 144.
[189] W. Zhang, T. Yang, D.M. Huang, K. Jiao, Chin. Chem. Lett. 19 (2008) 589.
[190] Z. Wang, Y. Yang, J. Li, j. Gong, G. Shen, R. Yu, Talanta 69 (2006) 686.
[191] M.H. Asif, S.M.U. Ali, O. Nur, M. Willander, C. Brännmark, P. Strålfors, U.H. Englund, F. Elinder, B. Danielsson, Biosens. Bioelectron. 25 (2010) 2205.
[192] J. Zhao, D. Wu, J. Zhi, Bioelectrochemistry 75 (2009) 44.
[193] S. Park, K. Cho, S. Kim, Microelectron. Eng. 88 (2011) 2611.
[194] J.M. Lee, G.-R. Xu, B.K. Kim, H.N. Choi, W.-Y. Lee, Electroanalysis 23 (2011) 962.
[195] N.T. Loan, L.M. Quynh, N.X. Dai, N.N. Long, Int. J. Nanotechnol. 8 (2011) 300.
[196] Y. Teng, X. Zhang, Y. Fu, H. Liu, Z. Wang, L. Jin, W. Zhang, Biosens. Bioelectron. 26 (2011) 4661.
[197] S. Siddiquee, N. Yusof, A. Salleh, S. Tan, F. Bakar, Microchim. Acta 172 (2011) 357.
[198] J. Xu, C. Liu, Z. Wu, Microchim. Acta 172 (2011) 425.
[199] A. Dorfman, N. Kumar, J.-i. Hahm, Langmuir 22 (2006) 4890.
[200] B. Haghighi, S. Bozorgzadeh, Talanta 85 (2011) 2189.
[201] A. Choi, K. Kim, H.-I. Jung, S.Y. Lee, Sens. Actuat. B: Chem. 148 (2010) 577.
[202] J.A. Hagen, S.N. Kim, B. Bayraktaroglu, K. Leedy, J.L. Chávez, N. Kelley-Loughnane, R.R. Naik, M.O. Stone, Sensors-Basel 11 (2011) 6645.
[203] C.-T. Lee, Y.-S. Chiu, S.-C. Ho, Y.-J. Lee, Sensors-Basel 11 (2011) 4648.
[204] A.F. Collings, F. Caruso, Rep. Progr. Phys. 60 (1997) 1397.
[205] Z. Zhang, H. Chen, J. Zhong, Y. Chen, Y. Lu, International Frequency Control Symposium and Exposition, 2006 IEEE, Miami, FL, 2006, p. 545.
[206] K. Länge, B. Rapp, M. Rapp, Anal. Bioanal. Chem. 391 (2008) 1509.
[207] G.S. Calabrese, H. Wohltjen, M.K. Roy, Anal. Chem. 59 (1987) 833.
[208] C.A. Flory, R.L. Baer, IEEE 1987 Ultrason. Symp. (1987) 313.
[209] S. Shiokawa, T. Moriizumi, Jpn. J. Appl. Phys. Part 1-Regular Pap. Short Notes Rev. Pap. 27 (1988) 142.
[210] G. Wingqvist, Surf. Coat. Technol. 205 (2010) 1279.
[211] Z. Yan, Z. Song, W. Liu, H. Ren, N. Gu, X. Zhou, L. Zhang, Y. Wang, S. Feng, L. Lai, J. Chen, Appl. Surf. Sci. 253 (2007) 9372.
[212] Z. Yan, X.Y. Zhou, G.K.H. Pang, T. Zhang, W.L. Liu, J.G. Cheng, Z.T. Song, S.L. Feng, L.H. Lai, J.Z. Chen, Y. Wang, Appl. Phys. Lett. 90 (2007) 143503.
[213] R. Gabl, H.D. Feucht, H. Zeininger, G. Eckstein, M. Schreiter, R. Primig, D. Pitzer, W. Wersing, Biosens. Bioelectron. 19 (2004) 615.
[214] A. Dickherber, C.D. Corso, W.D. Hunt, Sens. Actuat. A: Phys. 144 (2008) 7.